5-2019

Feedforward and Feedback Signals in the Olfactory System

Srimoy Chakraborty
University of Arkansas, Fayetteville

Feedforward and Feedback Signals in the Olfactory System

A dissertation submitted in partial fulfillment
of the requirements for the degree of
Doctor of Philosophy in Physics

by

Srimoy Chakraborty
University of Calcutta
Bachelor of Science in Physics, 2008
University of Arkansas
Master of Science in Physics, 2015

May 2019
University of Arkansas

This dissertation is approved for recommendation to the Graduate Council.

_____
Woodrow Shew, Ph.D.
Dissertation Director

_____
Wayne J. Kuenzel, Ph.D.
Committee Member

_____
Jiali Li, Ph.D.
Committee Member

_____
Pradeep Kumar, Ph.D.
Committee Member

Abstract

The conglomeration of myriad activities in neural systems often results in prominent oscillations. The primary goal of the research presented in this thesis was to study effects of sensory stimulus on the olfactory system of rats, focusing on the olfactory bulb (OB) and the anterior piriform cortex (aPC). Extracellular electrophysiological measurements revealed distinct frequency bands of oscillations in OB and aPC. However, how these oscillatory fluctuations help the animal to process sensory input is not clearly understood. Here we show high frequency oscillations in olfactory bulb carry feedforward signals to anterior piriform cortex whereas feedback from the aPC is predominantly carried by lower frequency oscillations. Similar frequency multiplexing of feedforward and feedback signals has been observed in other sensory systems, but our work is the first to show this in the olfactory system. We also pharmacologically manipulated inhibition in the OB. We found that weaker OB inhibition made the feedforward and feedback signal stronger whereas stronger inhibition resulted in a weaker feedforward and feedback signals. Our observations support hypotheses derived from predictive coding theory which suggests that low frequency inhibitory feedback may make coding more efficient by suppressing response to predictable sensory input. Our work, together with similar observations in other sensory brain regions, suggests that frequency-specific flow of information is a general principle of the sensory systems in the mammalian brain.

In a second project with entirely different goals, we developed a new experimental system for doing closed-loop control of neural activity in motor cortex of mice. We present preliminary results and discuss future directions for this second project.

Contents

Introduction 1
Overview of electrophysiology, oscillations, and connectivity 6
Experimental Methods 7
Subjects 7
Anesthesia 8
Double tracheotomy surgery. 8
Olfactory stimulation 9
Electrophysiology 10
Pharmacology 11
Data Analysis Methods 12
Basic time series 12
Power spectral density 13
Measuring directed interactions 24
Coherence and PLV 25
Granger causality 28
Results 37
Power spectra 37
Granger spectra 39
Effects of manipulating OB inhibition 41
Discussion 42
2nd Project: Optogenetic Feedback Control Pilot Project 44
Overview 44
Optogenetic stimulation and closed loop feedback control 45
Experimental Methods 47
Subjects 47
Anesthesia and surgery 47
Electrophysiology 48
Optical stimulation 48
Control algorithm 49
Results 52
Conclusions 56
Bibliography 57
Appendix 61

Introduction

One of the longest-standing goals in brain science is to determine how the activity of neurons in the brain represents the external world. In other words, how does information impinging on our senses get encoded in the brain. In this thesis, we study the sense of smell and how olfactory stimuli are represented in the olfactory system of rats.

In recent years a new way of interpreting how the brain encodes sensory input has emerged; this new approach is referred to as 'predictive coding'. Before explaining what predictive coding means, let us first discuss the more traditional view of sensory coding. Traditionally, the neural response to sensory input is thought to be determined almost entirely by features of the sensory input. Typical experiments involve presenting repeated trials of the same sensory input and then measuring the average neural response. Examining differences in average response for different sensory stimuli is then interpreted as revealing the sensory coding scheme.

In the view of predictive coding, in contrast, the neural response to sensory input is due to not only the features of the sensory input, but also the internal state of the brain when the sensory input arrives. More specifically, predictive coding supposes that the brains maintains an internal model of the outside world which provides a prediction of what sensory input it is expecting next (Shipp, 2016). According to predictive coding theory, the neural response depends both on the stimulus and how well the stimulus matches the prediction which the brain makes. The predictions made by the internal models in the brain are then updated continuously based on the accumulation of new evidence from sensory input (Friston, 2010). Although this school of thought is relatively new in the context of neuroscience, the idea dates back with its philosophical ethos from the times of Plato. In the last century, this idea was very clearly expressed by Hermann von Helmholtz in his book "Treatise on physiological optics." (Helmholtz, 1924).One rationale for predictive coding comes from examining the anatomy of the brain. The neurons in sensory systems do not simply relay sensory signals in one direction (feedforward) from the sensory organs to the higher levels of the brain. Rather, sensory signals are

processed by feedforward *and feedback* interactions among multiple brain areas between the sensory periphery and higher cortical areas. Here we consider “low-level” areas of the sensory system to be those closest to the sensory organs that receive the input and “high-level” areas to be those that receive input from the low levels, but not directly from the sensory organs. Signals transmitted from low levels to high levels are termed “feedforward”, while signals transmitted from high to low levels are termed “feedback”. The existence of these feedback interactions strongly suggest that the neural response to sensory input should be due to the combination of sensory input and feedback signals from higher areas. An important question is how do inter-areal interactions contribute to multi-level sensory processing and fit in the predictive coding scheme. According to predictive coding theory, feedback signals of the sensory system carries predictions of the external world, based on the internal model. The low-level areas receive these feedback predictions from high levels and the actual inputs from sensory stimulus. The difference between the prediction and the sensory input gives rise to the “error” (the poorly predicted part of the sensory input) which is considered as the ‘newsworthy’ part. This error constitutes the feedforward signal. The error propagating up changes the internal model at the higher levels. This is essentially similar to optimizing the model to reduce the error. Predictive coding is conceptually appealing and quantitatively sensible, but the actual biological mechanisms and detailed neural pathways that might implement the predictive coding algorithm are often debated.

One of the implications of the predictive coding theory (Friston, 2010; Shipp, 2016; Spratling, 2017), is that feedback from higher levels suppresses certain feedforward signals coming from lower levels. The strategy is only those parts of the sensory signal which are surprising or “newsworthy” enough will be passed effectively to the higher levels. This helps the system to spend less resources for less important parts of the signals. Thus, according to predictive coding, feedback from the higher to the lower parts of the sensory system should be inhibitory.

Therefore, one biological mechanism that could be important for predictive coding is that inhibitory neurons may play an important role in mediating feedback signals.

The predictive coding theory also suggests that feedforward and feedback signals could have distinctly different character of temporal fluctuations. It is very common to observe that the collective activity of large neural populations exhibit highly complex temporal fluctuations, sometimes with clear periodic oscillations with particular frequencies, sometimes with more broadband fluctuations. Theory suggests that feedforward signals (prediction errors) will contain more high frequency fluctuations compared to feedback signals (predictions) (Andre M. Bastos et al., 2012).This leads to an experimentally testable hypothesis: the feedforward signals from lower levels in a sensory system to higher levels should have more high frequency content and feedback signals will have more low frequency content.

This hypothesis has been confirmed across various studies in different cortical areas. All of these point to the fact that feedforward signals are carried by high frequency gamma oscillations (30 – 100 Hz), while feedback signals are carried by low frequency oscillations (10 – 20 Hz) (A.M. Bastos et al., 2015; André Moraes Bastos et al., 2015; Colgin et al., 2009; Fontolan, Morillon, Liegeois-Chauvel, & Giraud, 2014; Jensen, Bonnefond, Marshall, & Tiesinga, 2015; Michalareas et al., 2016a; Richter, Thompson, Bosman, & Fries, 2017; van Kerkoerle et al., 2014). In the visual cortex (V1 and V4) (A.M. Bastos et al., 2015; André Moraes Bastos et al., 2015; Jensen et al., 2015; Michalareas et al., 2016a; Richter et al., 2017; van Kerkoerle et al., 2014) it was found that the feedforward signals were carried by the gamma frequencies whereas the feedback were carried by the lower alpha beta band. In the auditory cortex (A1 and AAC) (Fontolan et al., 2014) the feedforward was carried by gamma and feedback by the lower delta and beta frequencies. In the hippocampal network also, high and low frequency gamma signals are observed which are thought to be the feedforward and feedback signals (Colgin et al., 2009) All the above studies have one thing in common and it suggests high frequency feedforward and low frequency feedback oscillatory behavior might be a ramification of a more

general principal of the interactions of a complex sensory system. But this has not been tested in the olfactory system, or on any sensory system that includes regions outside of the cortex. The primary work presented in this thesis tests this idea in the olfactory system consisting of the olfactory bulb (OB), which receives input from sensory neurons in the nose and is outside the cortex, and the anterior Piriform Cortex (aPC), which receives input from OB and sends feedback to OB (Figure 1).

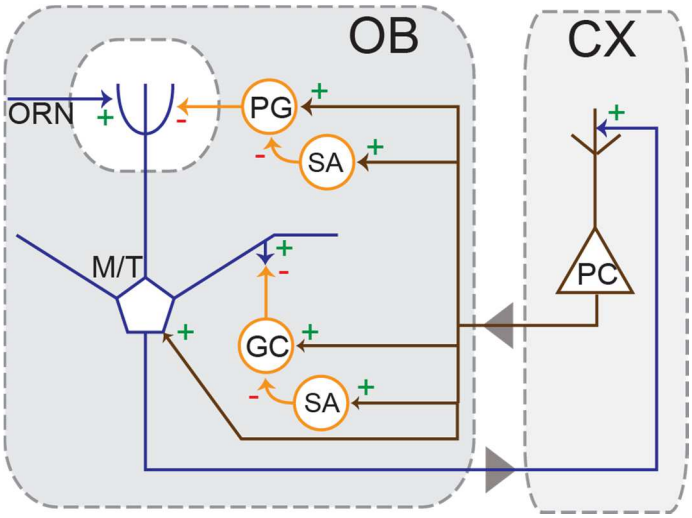

Figure 1: The neural connections of the OB and the aPC.(+ sign implies excitatory influence whereas the – sign implies inhibitory influence) The mitral and the tufted cell (M/T) sends olfactory information to the pyramidal cells (PC) in the anterior piriform cortex (excitatory). The PC has its projections back to the Granule Cell (GC), the periglomerular cells (PG) and the short axon cells (SA) in the Granule cell layer and the Glomerular layer. The GC, PG, and SA cells are all inhibitory, which makes the effective influence from the aPC to the OB inhibitory.

There are a lot of previous studies concerning the oscillations of collective neural activity in the OB and the aPC in rodents (Gelperin, 2006; Kay et al., 2009; Neville & Haberly, 2003). The oscillations in the OB and aPC are most prominent in two distinct frequency bands; one in higher frequencies near 40-60 Hz, one in lower frequencies near 10-20 Hz. Also it is well established that cortical feedbacks from aPC to OB largely targets inhibitory neurons in OB as illustrated in Figure 1 (Boyd, Sturgill, Poo, & Isaacson, 2012; Markopoulos, Rokni, Gire, & Murthy, 2012; Mazo, Lepousez, Nissant, Valley, & Lledo, 2016; Oswald & Urban, 2012).

All the above facts suggest that the olfactory system could implement predictive coding and more specifically could exhibit frequency-specific feedforward (fast excitatory) and feedback (slow inhibitory) oscillatory interactions. To test this hypothesis, we simultaneously recorded the local field potentials from the OB and the aPC of an anaesthetized rat during olfactory stimulation. As we will explain in greater detail in following sections, we confirmed our hypothesis. In brief, we found that the feedforward signal was carried by oscillatory signals with frequency near 50 Hz while the feedback signals were carried by slower oscillations around 20 Hz. This shows that frequency division multiplexing of feedforward and feedback signals generalizes across more sensory systems than previously thought and suggests that predictive coding may play a role in olfactory information processing.

Overview of electrophysiology, oscillations, and connectivity

There are many experiment techniques for measuring brain activity. The technique used in this thesis is electrophysiology, which entails measuring the voltage fluctuations generated by the brain activity. There are several kinds of important electrophysiological signals, including electroencephalogram (EEG), electrocorticogram (ECoG), the local field potential (LFP), and intracellular patch-clamp recordings. EEG is a noninvasive method and is recorded from the electrodes on the scalp whereas the LFP's are recorded by tiny electrodes inserted inside the brain. EEG, ECoG, and LFP are based on electrodes that are extracellular, whereas, patch clamp recordings measure the voltage difference across the cell membrane of a single neuron. Here we will mostly talk about the Local Field Potentials (LFPs). As the name suggests it's the voltage (field potential) created by a local ensemble of neurons. Various ionic currents flow in the tissue, and we measure its potential (field potential) with respect to (w.r.t) a standard point. The field reflects the weighted sum of all the transmembrane currents in all the cells in an influence zone (Kajikawa & Schroeder, 2011a). Some of the currents are due to action potentials fired by local neurons and some are due to synaptic inputs to local neurons (distant action potentials). However, it's often debated how much local it is. The degree of locality can depend on the region of the brain as well as the frequency of the activity. The V1 showed that 95% of the influence of a recorder comes from neurons within 250 μm radius (Katzner et al., 2009) whereas other areas show it can be over few mms (Kajikawa & Schroeder, 2011b). High frequency LFP (~10-100 Hz) are relatively local, while low frequencies (~0.1 – 1 Hz) tend to be correlated across greater distances. So LFPs are probably best understood when they are looked upon as a mixture of local and volume conducted potentials. Despite the controversies, it is clear that the LFPs represent collective activity of many neurons and LFP remains one of the very important tools very to understand the brain (Buzsáki, Anastassiou, & Koch, 2012). Once the LFP is recorded its processed before analysis. These preprocessing steps includes but is not limited to the following. I) Data from bad electrodes are eliminated. II) It can be filtered

according to needs (for example to get spikes we filter out the low frequency content of our recordings whereas to get LFP we filter out the high frequency part of the recordings.). This process includes all the steps required from acquiring and before analyzing the data and it depends mainly on what kind of analysis we are doing.

Since the first pioneering measurements of electrical brain activity in humans by Hans Berger in 1924, it was noticed that this electrical activity is often oscillatory with distinct frequencies. The frequency analysis (power spectral analysis) is often used to reveal the important frequencies/oscillations present in the recordings. In OB of rodents, there are 3 distinct bands of oscillatory rhythms, which are traditionally called theta (~4-12 Hz), beta (~13-34 Hz) and gamma (~40-90 Hz). These distinct bands of oscillations however differ from animal to animal and they get activated during different kinds of situations and carries different messages (Kay et al., 2009). However, it is not well understood how interactions between the OB and the aPC are related to these different frequencies.

This brings us to the issue of connectivity. Different brain regions often exhibit strongly correlated LFP oscillations, which suggests that the different regions are connected anatomically. Since it is difficult to directly measure the anatomical connections among brain regions and relatively easy to measure LFP oscillations, researchers commonly use LFP correlations as a measure of “functional connectivity”. There are many connectivity analyses some phase based and some power based. Here we will be using the Granger causality to understand how the influences are flowing bidirectionally and how that's influenced by stimulus.

Experimental Methods

Subjects

All procedures were carried out according to the recommendations of the Guide for the Care and Use of Laboratory Animals of the National Institutes of Health and was approved by

University of Arkansas Institutional Animal Care and Use Committee (protocol #12025). Only male rats were studied (n = 11, 328±54 g; *Rattus Norvegicus*, Sprague-Dawley outbred, Harlan Laboratories, TX, USA). Animals were kept in the animal facilities with standard care. They were housed in a cage of controlled humidity (60%) and temperature (23°C) with 12 hr light-dark cycles. The experiments were performed in the light phase.

Anesthesia

First the animal is anesthetized using vaporized form of isoflurane inhalation. Then it is maintained with urethane (1.5 g/kg body weight dissolved in saline, intraperitoneal injection). Dexamethasone (2 mg/kg bw) and atropine sulphate (0.4 mg/kg bw) were administered intraperitoneally before performing the surgery and were applied till the experiment ends at an interval of 90 mins.

Double tracheotomy surgery.

Double tracheotomy surgeries were performed on the rodents to redirect the breath of the animal allowing the experimenter to precisely control the airflow through the nose without interference from the breath (Gautam & Verhagen, 2012). A Teflon tube (OD 2.1mm, upper tracheotomy tube) was put 10 mm into the nasopharynx through the tracheal cut. This tube was used for delivering the odors retronasally. Through the caudal end another Teflon tube (OD 2.3 mm, lower tracheotomy tube) was inserted. This allows normal breathing. The tubes were sealed with surgical thread and cyanoacrylate glue with the tissues. Local anesthetic (2% Lidocaine) was applied during these procedures. To keep the rats comfortable throughout the surgery and the recording period their body temperature was controlled by a thermal pad (thermostatically controlled) at 37°C.

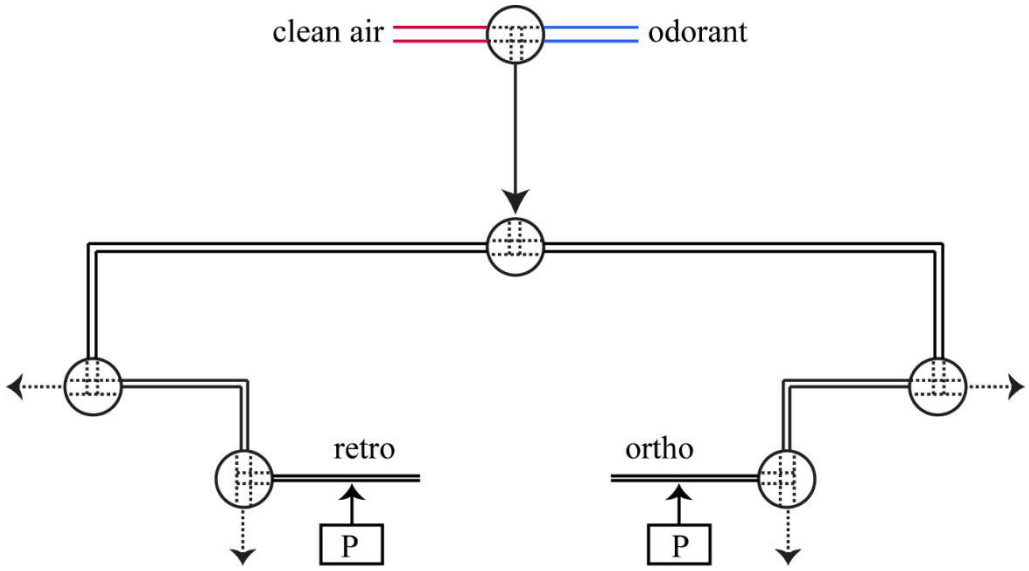

Figure 2: A schematic cartoon showing the tubing arrangements for delivering the odors ortho- and retronasally. The retro tube was put 10 mm into the nasopharynx through the tracheal cut. The ortho tube was inserted into the nostril of the mouse. Circles are switchable valves, which were changed manually to control the type of stimulus. A pressure sensor P was used for both the ortho and retro stimulus which measured the flow resistance to control the stimuli.

Olfactory stimulation

The data analysis presented in this thesis is not focused on differences between different types of olfactory stimulation. However, the original experiments were designed to study the differences between 'orthonasal' and 'retronasal' stimulation. Orthonasal means the odorant enters the nasal cavity through the nostrils in the front of the nose. Retronasal means the odorant stimulus enters via the throat at the back of the nasal cavity. The differences in neural response to these different types of stimuli are subtle, so we combined both types of stimuli together in the analysis presented later in this thesis. Nonetheless, for completeness, we describe here how these different stimuli were generated.

Orthonasal odors were delivered through a Teflon tube that was inserted into the right nostril. The left nostril was closed by suturing. The upper tracheotomy tube was used to deliver odor retronasally. The flow rate was carefully adjusted and was kept equal to the flowrate of the sniffing awake rats (L.Youngentob, 1987). The valves operating to deliver the odor was

controlled by a LabVIEW program. Two odorants Hexanal (Hexa) and Ethyl Butyrate (EB) were used. They were both delivered orthonasally as well as retronasally. So, four different kind of stimuli were applied. Trials comprised of 10 of these odor puffs or stimuli. Each stimulus was a puff of constant strength for 1 sec and a gap of 30 secs was kept before the next puff. A time gap of 2 to 3 secs were kept between 2 successive trials. Each kind of stimulus were presented 3 to 5 times. Below in the figure (3) we see pulses were almost constant though there was a little dip but the effect of that can be safely ignored. The stimulus was simultaneously recorded with the LFP in another channel of the data acquisition system.

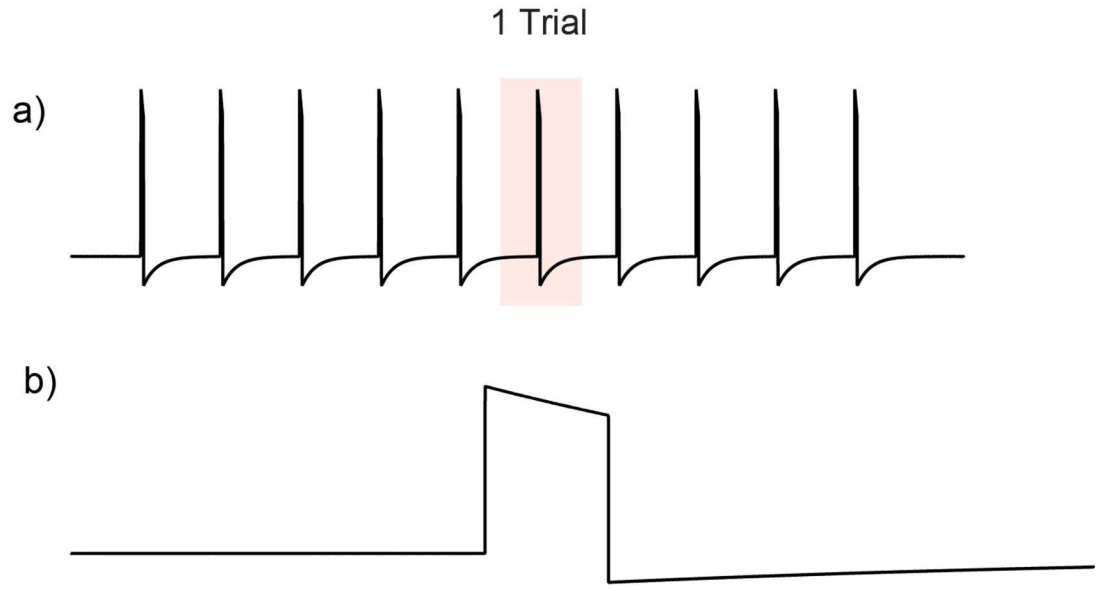

Figure 3 –a) Recordings from the 65th channel which represents the stimulus control voltage (the voltage is high when the valve was open allowing odorized air flow through the nose). There are 10 stimuli in 1 trial. b) We zoomed in one of the stimuli. Each stimulus is 1 second in duration.

Electrophysiology

To measure LFPs simultaneously from OB and aPC two different sets of 32-channel microelectrode arrays (MEAs) (OB: A4x2tet, 4 shanks x 2 iridium tetrodes per shank, inserted 400 μm deep from dorsal surface; aPC: Buzsaki 32L, 4 shanks x 8 iridium electrode sites per shank, 6.5 mm deep from dorsal surface; NeuroNexus, MI, USA) were used. Voltages were

measured with respect to a ground. In our case the ground was an AgCl pellet. It was placed close to the MEA's and it touched the exposed brain surface. It was covered with gel foams soaked in artificial cerebrospinal fluid (acsf). Care is taken so that they don't get dry during the time of recording, so we applied acsf after every half an hour or as required to keep the exposed surface moist. The idea is that the MEA's and the ground are in the same fluidic bath. Voltages were recorded (digitized) at a 30 kHz sample rate (Gautam, Hoang, McClanahan, Grady, & Shew, 2015) using Cereplex + Cerebus, Blackrock Microsystems (UT, USA).

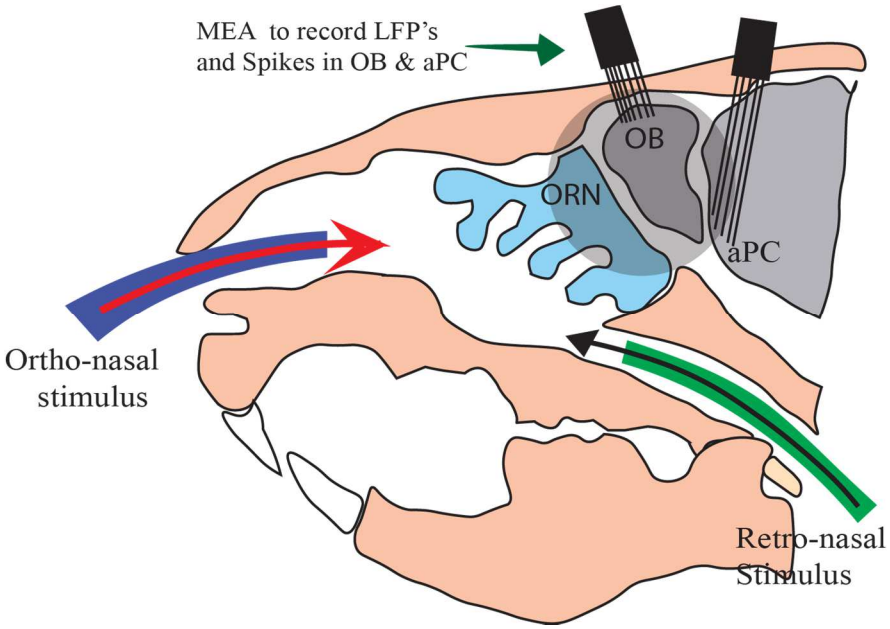

Figure 4 : A schematic cartoon showing the relative position of the OB and the aPC with the MEA's in them. Also showing the ortho and the retro nasal odor delivery system.

Pharmacology

We recorded the ongoing and the stimulus evoked activities from the rats under no drug conditions initially. Then we applied drug (20 μM bicuculline methiodide (5 rats) or 20 μM Muscimol (4 rats)). Topically to the OB exposed surface by gel foam pieces soaked with the drug. For one rat we applied only one kind of drug after the no drug set of data was recorded. And we repeated a set of trials similar to the no drug conditions. After recording the drugged

cases we tried to wash the drug with drug-free gel foams to test if the activity returns to state before drug was applied. For bicuculline we found the activities got reverted to its no drug conditions however for Muscimol the activity didn't recede to its previous no drug state.

Data Analysis Methods

In this section we step by step explain how we measure connectivity starting from power spectral density, what are the necessary steps and what kind of connectivity analysis best suit our purpose. We will explain the statistical significance part of our analysis in the results section.

Basic time series

We simultaneously record from both the OB and the aPC during both the ongoing activity (with no olfactory stimulus) and the stimulus-evoked activity. Here we show example recordings from both OB and aPC (Figure 5). We filter out the very low frequencies (< 3 Hz) with a high-pass filter and the line frequencies (60 Hz) by a notch filter.

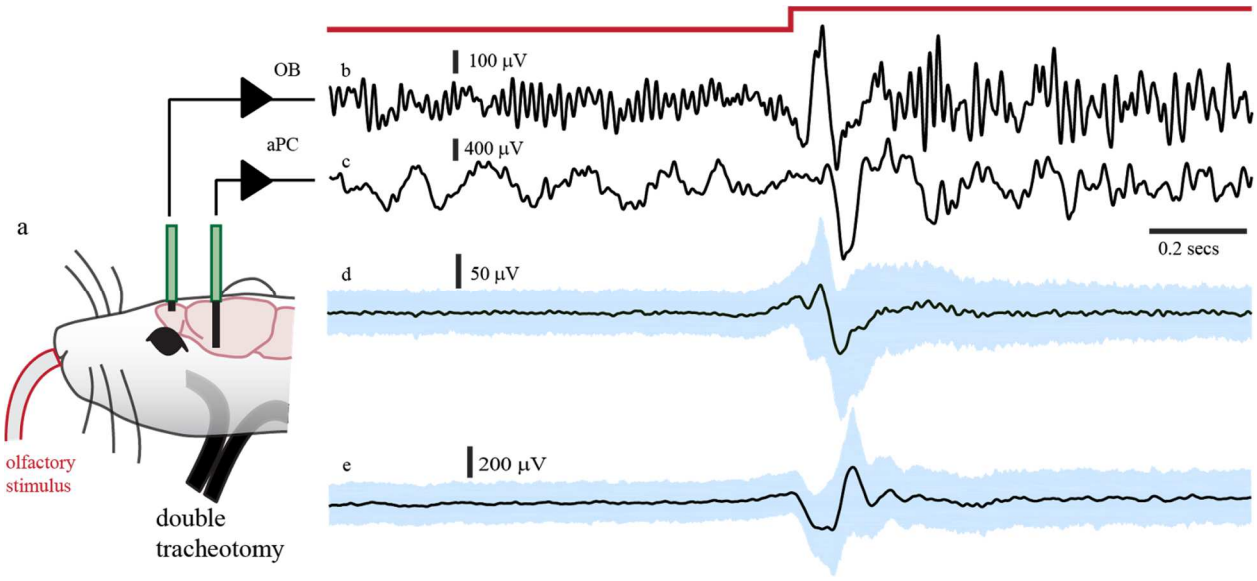

Figure 5: a) A schematic diagram of the experimental setup showing simultaneous recording from the OB and the aPC. b) & c) LFP from a single trial (animal no 10, trial=4 and 1st stimulus) of OB and aPC averaged over the electrodes. d) & e) LFP averaged over many trials across all animals, trials and stimuli for OB (d) and aPC (e). (The blue patch represents the interquartile range of variability across trials). The red line at the top shows a step increase at the onset of the stimulus.

All filters were applied using the Matlab 'filtfilt' function to avoid phase shifts, which can be very important for assessment of Granger causality (described below). Also, we omitted the recordings from the dead channels (OB: [1 ,23] and for aPC: [11,12, 17, 18, 30, 31]) in all our analysis unless otherwise stated.

In the Figure (5) we can see the oscillations in the LFP clearly and how they change with the stimulus in the later half (when the stimulus is applied) in both the OB and the aPC. Next, we sought to measure the frequency content of the LFP's. One thing about the LFPs specially if we want to know how they behave with respect to certain stimuli we need to know the event related potentials or ERPs. The idea is LFPs that are recorded (in a single trial) reflects the neural activity accompanied by some other activities which are not related to the applied stimulus. So, averaging over multiple trials one can hope the nonrelated events will cancel out whereas the related events (which are most of the time and phase locked with the stimulus) will get more pronounced. We get the ERP by averaging over multiple LFPs from different trials. Now if the LFPs (rather the evoked part of the LFP) are not time and phase locked the oscillation is not pronounced in the ERP. If we have a power spectral density of a single trial and average over the power spectral densities (PSD) of the single trials it will show up there. The order should be kept in mind.

Power spectral density

PSD of a single trial and then average over the PSDs ≠ PSD of average of the trials

Most of our calculations for the power spectrum is obtained by the left-hand side of the above inequality that is the average of the power spectral densities of the single trials.

We see in figure 5 a very high amplitude low frequency part of the ERP in both the OB and the aPC. This part drives the mean value above 0. Its very important to have 0 mean in our analysis. This kind of anomaly needs to be removed before we apply the tools of our analysis.

In our case we really didn't need to think about it as we were interested in a frequency much higher than this and we found the mean very close to 0 for most of the trials.

We used the complex Morlet wavelength analysis to get the spectral contents. The reason Morlet wavelet is chosen over the other methods for our analysis is because it gives the optimum temporal and frequency resolution. Let's explain this in a bit more detail. The popular method of Fourier transform gives us the frequencies in a time series. There are other methods like the Hilbert transform (Bruns, 2004) also. However, it's very difficult to locate from which times during the time series the different frequencies were prominent. So, if we have a window of 10 sec for our analysis and we do a spectral analysis (fast Fourier transform (fft)) and find some frequencies (let's say 10 Hz and 50 Hz) it's difficult to say when the 2 frequencies were elicited. There is a possibility that the 10 Hz signal was in the beginning and later there was the 50Hz signal but by this method there is no way of knowing that. In other words, we don't have the temporal resolution of the frequencies. Of course, we can tackle this problem by breaking up our data into sliding windows but if we make the window small we gain temporal precision but loose frequency resolution, so the crux of the problem remains. This is really a big issue not only in LFP's but also in many physiological recordings as most physiological recordings are not stationary, so the spectral content of the signal is changing with time and temporal resolution is important if our goal is to know how the spectral contents change with time. The kernel used for the standard Fourier transform is a continuous sinusoidal wave (which is non-localized as it spreads to infinity) whereas the kernel for this (Morlet wavelet) is localized. Here we show an example of a typical Morlet wavelet (in time domain) which is a sine wave enveloped by a gaussian. We change the width of the Gaussian envelope as much as we want to see the resolution in time. However instead of using a sine wave we would be using a complex representation of the sinusoidal wave and hence our wavelet would be complex. A typical

complex Morlet is given by $\frac{1}{s\sqrt{\pi}} e^{\frac{-t^2}{2s^2}} e^{i2\pi ft}$ where the complex wave is windowed by the gaussian envelope.

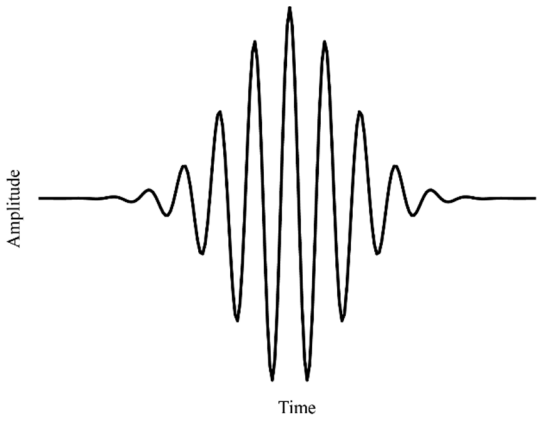

Figure 6: A typical morlet wavelet (cycles and width vary according to the need of the analysis)

Now the next question comes how we get the power spectrum from these wavelets. To do that we start convoluting the time series (LFP recordings) with our kernel which is the complex Morlet wavelets. Which is basically the dot product (element wise multiplication and sum) of the kernel and the time series. We must keep in mind the kernel and the time series should have the same sampling frequency.

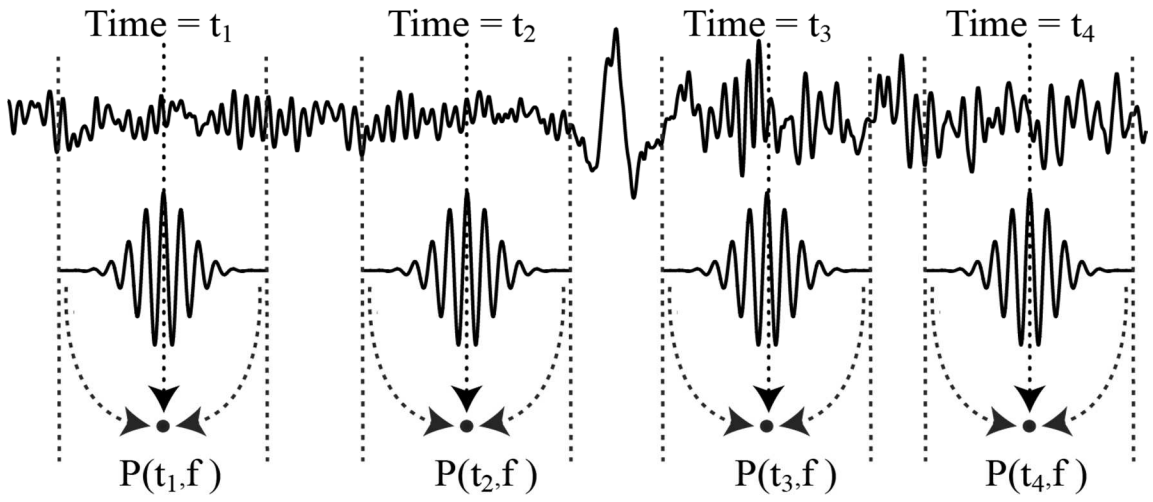

Figure 7: The shifting Kernel to convolute with the time series

So, we get the dot product of the kernel with the time series and we get a convoluted complex time series. The convoluted series is complex as our kernel is a complex Morlet wavelet. The amplitude of that gives the Power for the frequency of the wavelet at the time (t). The wavelet shown here has a frequency of 6 Hz (That is if we take the Fourier transform of our wavelet we will get a peak at about 6 Hz). So, we slide the wavelet and get the convoluted series for all the time points and then the power. In the above figure we have shown only 4 time points where we have got the power at frequency f (6 Hz) for time t_1, t_2, t_3 and t_4. We then change the frequency of our wavelet and repeat the same procedure for a different frequency. Likewise, we span the whole required frequencies to get the full power spectral densities for our LFPs.

Let us try the above with a sample time series (LFP from a single trial of animal no 10, trial=4 and 1st stimulus in OB, same as in Fig1). Let us try with 2 frequencies one in the beta range (20 Hz) and other in the gamma range (40 Hz).

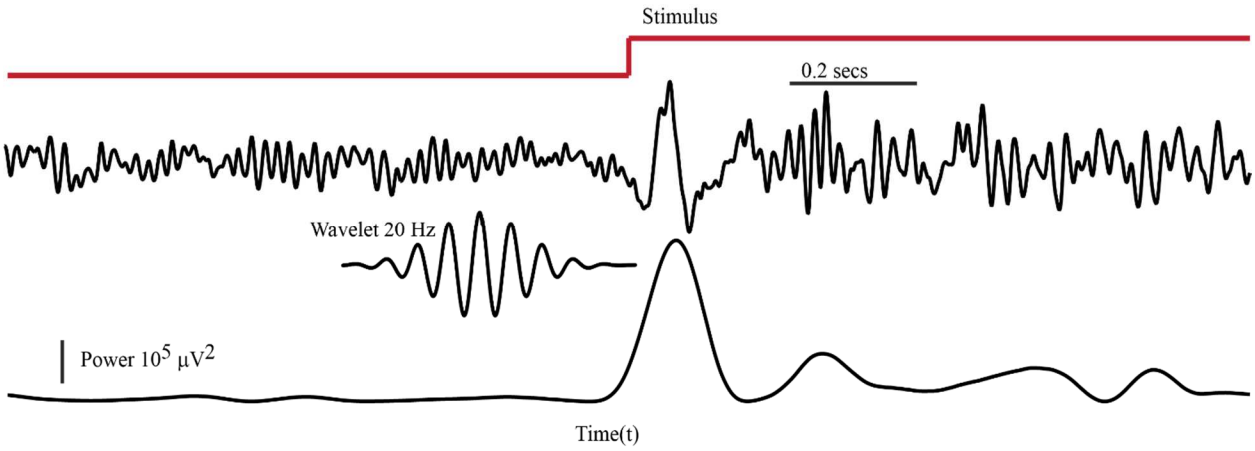

Figure 8: We obtained the power for the frequency 20 Hz using the wavelet as shown. We see an increase in power at the onset of the stimulus.

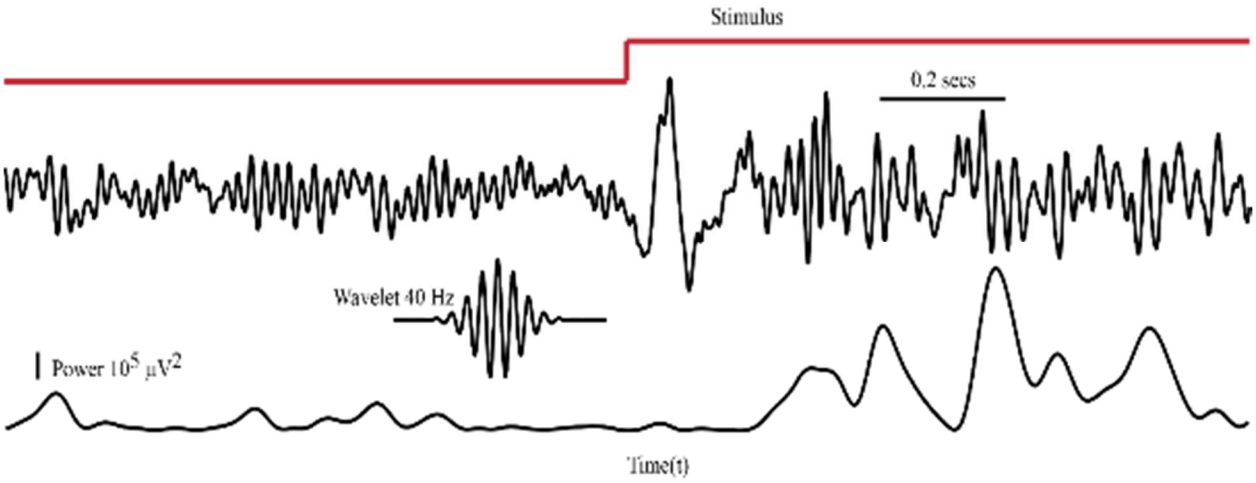

Figure 9: We obtained the power for the frequency 40 Hz using the wavelet as shown. We see an increase in power at the onset of the stimulus.

So, we see a change in power in both the frequencies at the onset of the stimulus. So now we would like to represent the power associated by all the frequencies (within our range of interest). However, before that we would like to see a less computationally expensive way to arrive at the same thing. Convolution in time domain is equivalent to multiplication in frequency domain.

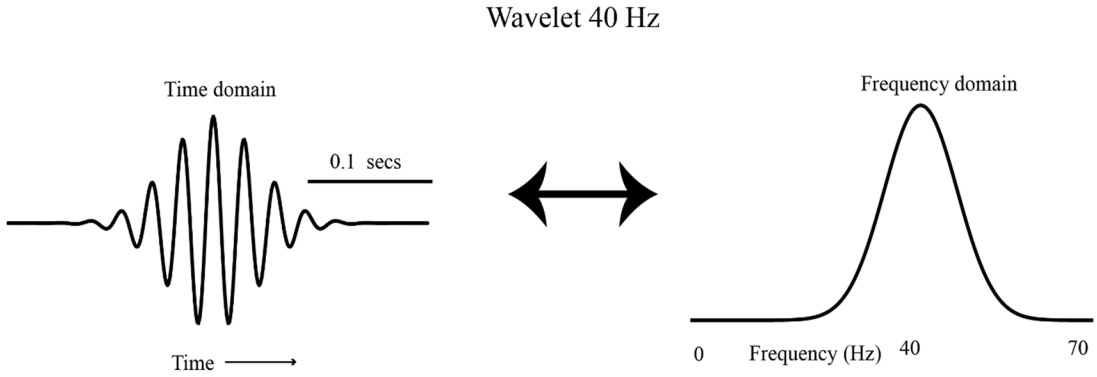

Figure 10: The time and frequency domain representations of the Morlet wavelet.

So, let's try this with our kernel, the wavelet and the time series (LFP recording). So first we take the Fourier transform of both and see the frequency components of them in the frequency domain. The wavelet we choose was 40 Hz (time domain picture in Fig 6) and the Fourier transform give us its picture in the frequency domain. They are equivalent information in the time and the frequency domain. We see it has a peak 40 Hz power in the frequency domain and that's expected as the wavelets have a gaussian envelope over a 40 Hz oscillation.

Now we must find out the frequency representation of the time series. Once we get that we multiply the spectrums, since convolution in the time domain is equivalent to multiplication in the frequency domain. The inverse Fourier transform on this resultant series will bring us back to the same series which we should have got by convolution. The process is shown in the example below in Figure 11. So, we multiplied the Fourier transform of the wavelet (Fig 11a) with the Fourier transform of the time series (Fig 11b) to get the resultant series (Fig 11c). An inverse Fourier transform on this series should give us back the same series that we got from convolution in time.

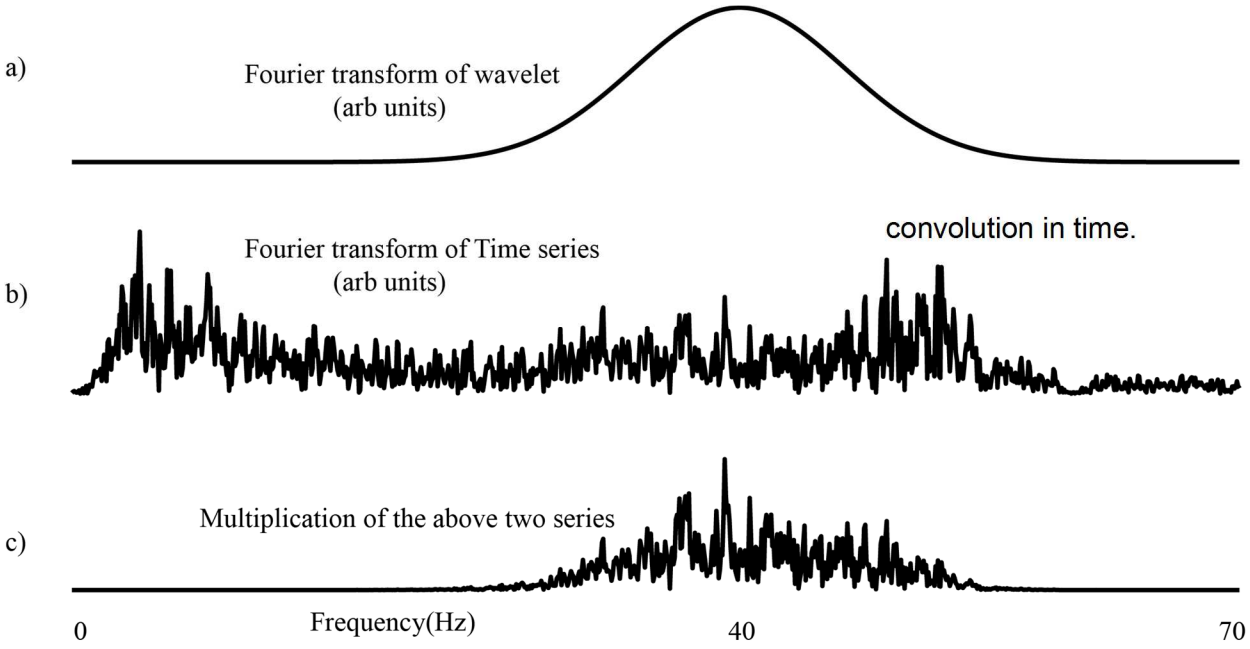

Figure 11: Multiplication in the frequency domain

And we can recover the power from this one too. We see below (in figure 12) that the power we recovered is same as in the one with convolution in time (in figure 9). So, we see these 2 methods yield similar kind of results. However, the 2nd method is computationally less time consuming than the first one. Hence forth we will use this method only to find the power spectral

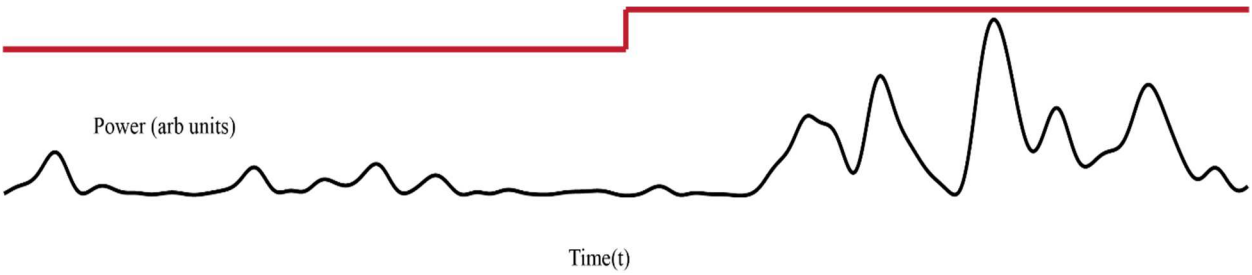

Figure 12: The power spectrum obtained by the inverse Fourier transform method.

density unless otherwise stated. We found the power for 100 frequencies uniformly(linearly) spaced in between 3 Hz to 100 Hz to get our power spectral density.

For the wavelet the number of cycles is an important feature. If we see our wavelet equation by $\frac{1}{s\sqrt{\pi}} e^{\frac{-t^2}{2s^2}} e^{i2\pi ft}$ the s which also controls the spread of the wavelet is determined by the number of cycles. So s is defined as $s = \frac{n}{2\pi f}$ where n is the number of cycles. So, let's see what happens when we change this parameter n. We created 2 wavelets of different cycles but having same central frequency 20 Hz and we see it in both time and frequency domain in Figure 13)

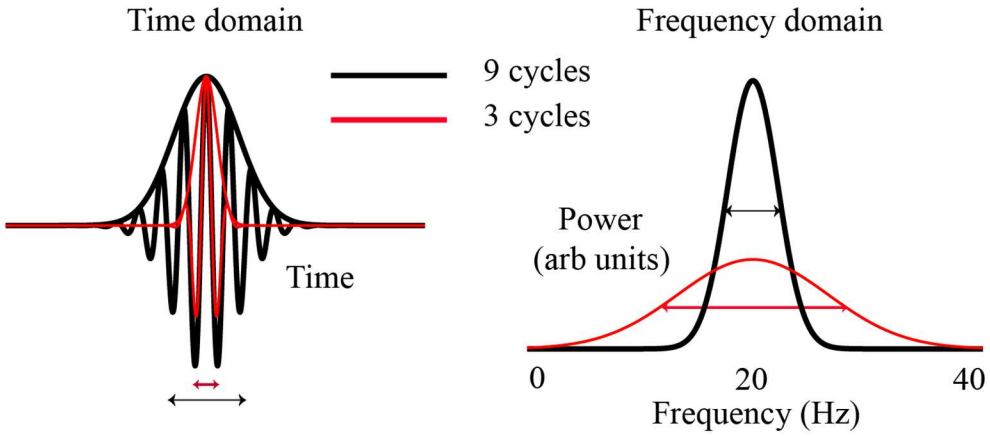

Figure 13: Wavelet of 20 Hz in both time and frequency domain in different cycles.

We find for less number of cycles it spreads less in time domain but widens up in frequency domain whereas if number of cycles are more (9) we find it has a wider span in time domain, but it has sharpened up quite a bit in the frequency domain. This has a profound influence in choosing the number of cycles for our frequencies. The above finding implies that if we want a high frequency precision we should go for higher number of cycles whereas if temporal precision is our concern we should go for a smaller number of cycles. So, if some frequencies are elicited for a considerable amount of time, we can use a wavelet having large number of cycles since it will provide us with a better frequency resolution and we can afford it if we know things are not changing quickly and we don't require a very good temporal precision. However, if things are changing fast we might need to sacrifice some of our frequency precision by downscaling to a smaller number of cycles to get more precision in time as that will help us to detect more ephemeral events. So, there is no hard and fast rule to select the number of cycles for the wavelets but rather the decision is mostly guided by the requirement of the analysis or what question one need to answer. Let's see with one example from our data.

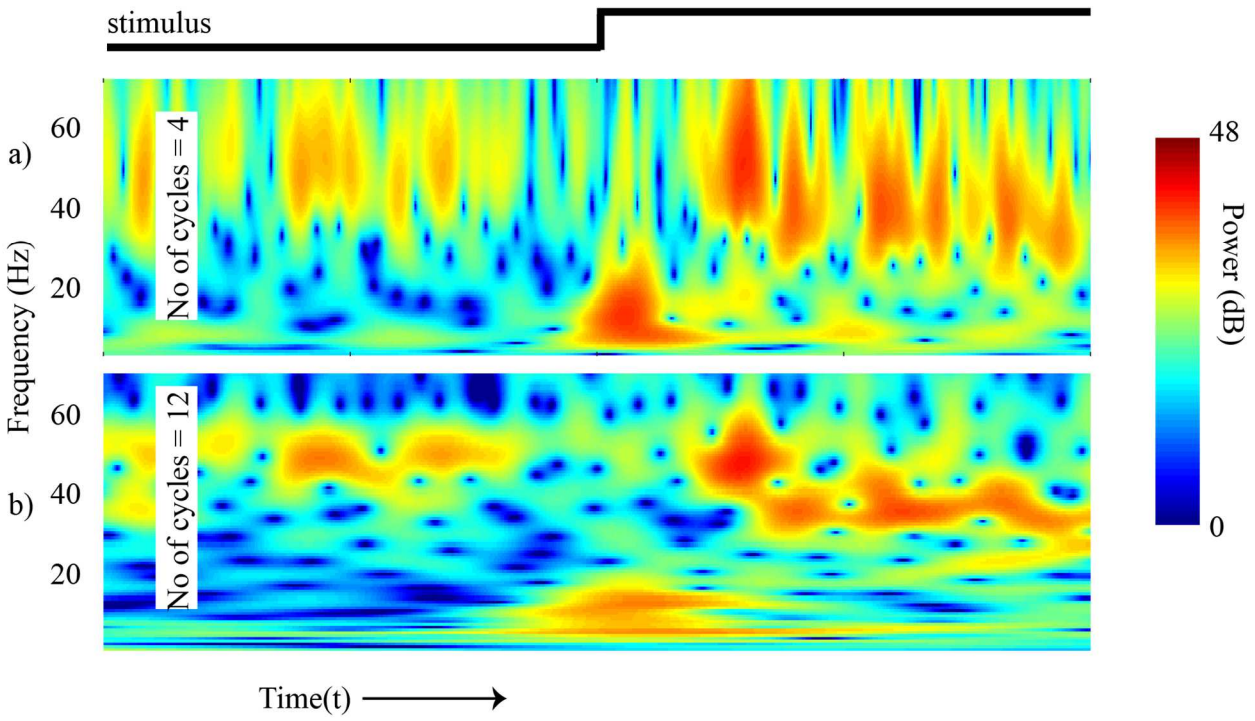

Figure 14: Power spectral density of the same time series for 2 cycle numbers a) 4 and b) 12

We have plotted the power spectral density for our data (animal no 10, trial=4 and 1ststimulus). It should be noted the units are in dB as it's the logarithmic value is taken instead of the actual value. Now we see over here that as expected the PSD with small number of cycles (4) has a high temporal precision. We can detect when the frequencies rise and falls but we cannot pinpoint to a particular frequency as its more stretched in the frequency axis. Now for the PSD computed with more number of cycles we see the evoked frequencies are not that stretched along the vertical axis which means we can say more clearly which frequency is evoked but its more stretched in the time axis which robs us some of our temporal precision and we cannot say as clearly as before exactly when it started. We must come up something in between these two extremities and our aim would be to extract the most possible information according to our need. Also, the full width at half maximum (FWHM) is a measure to understand the spread of a gaussian curve is also not the same for all frequencies (wavelet in the frequency domain). Here we have plotted the FWHM for a wavelet (in frequency domain) having a fixed number of cycles (number of cycles= 4). We see the FWHM increases as the frequency increases.

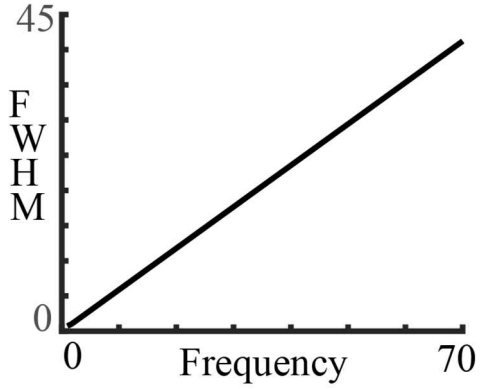

Figure 15: The change in width (precision of the frequency) given by FWHM for a fixed number of cycles with frequency

So, we used low number of cycles for lower frequencies and higher number of cycles for higher frequencies. We changed our number of cycles continuously as we changed the frequency of our wavelet. We changed the number of cycles from 3 to 12. Our lowest frequency wavelet has 3 cycles and our highest frequency wavelet has 12 cycles. Also, this increment from 3 to 12 is chosen to be logarithmic instead of linearly increasing them. We found our power spectral density with the help of these wavelets having varying cycles with frequency. One important and trivial thing is kept in mind that in time domain the wavelets should be long enough that it tapers to 0. We follow the above rule hence forth onwards to find different power spectral densities. We plot the same data as shown in Figure 14 (added with the simultaneous aPC spectrum also).

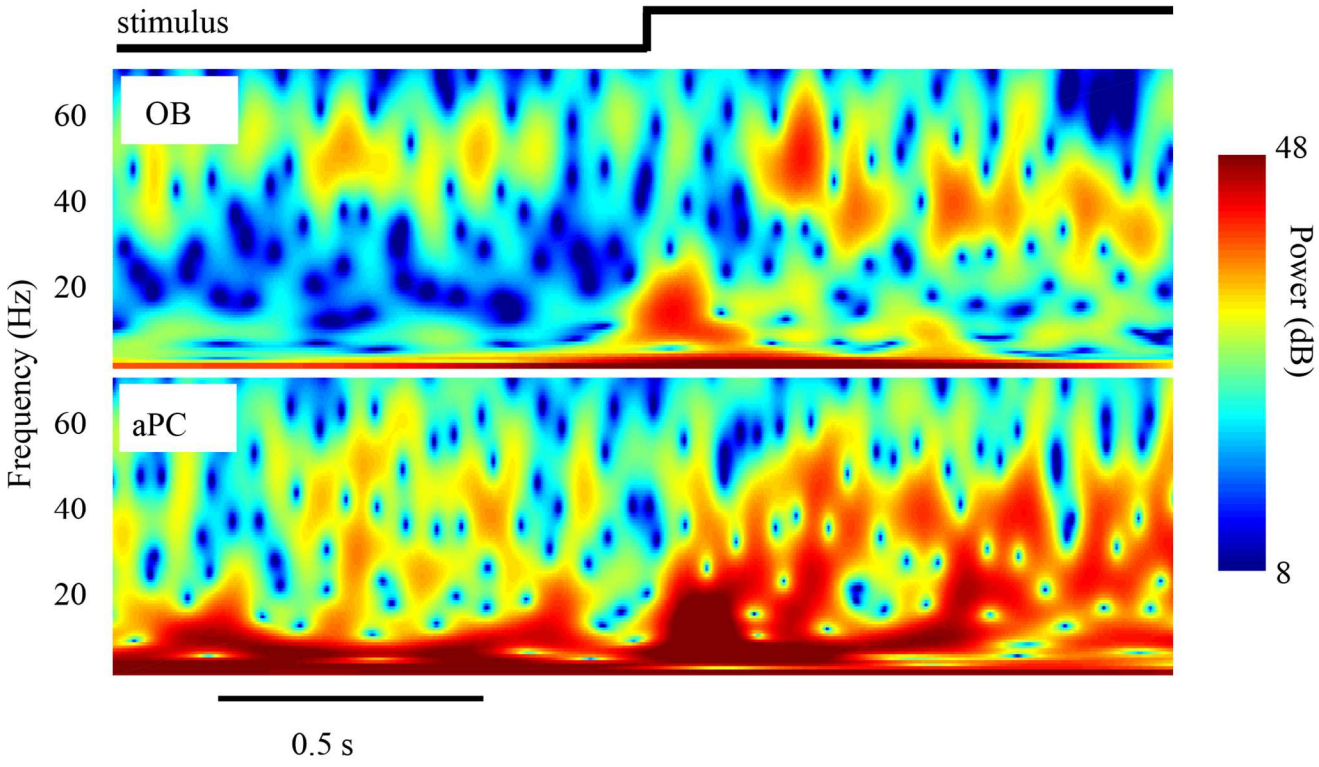

Figure 16: A single trial power spectral density(psd) of both the OB(top) and aPC(bottom).

If we see the PSD of OB (upper part of Fig 16) found by this method, we can see it meets a balance that we were talking about.

It has a fair precision in both frequency and time that we can see when the frequency is evoked and what are frequencies that are evoked. This PSD is obtained for a single trial. We can see the frequencies that are present. There were some gamma oscillations (about 50 Hz) present before the stimulus.

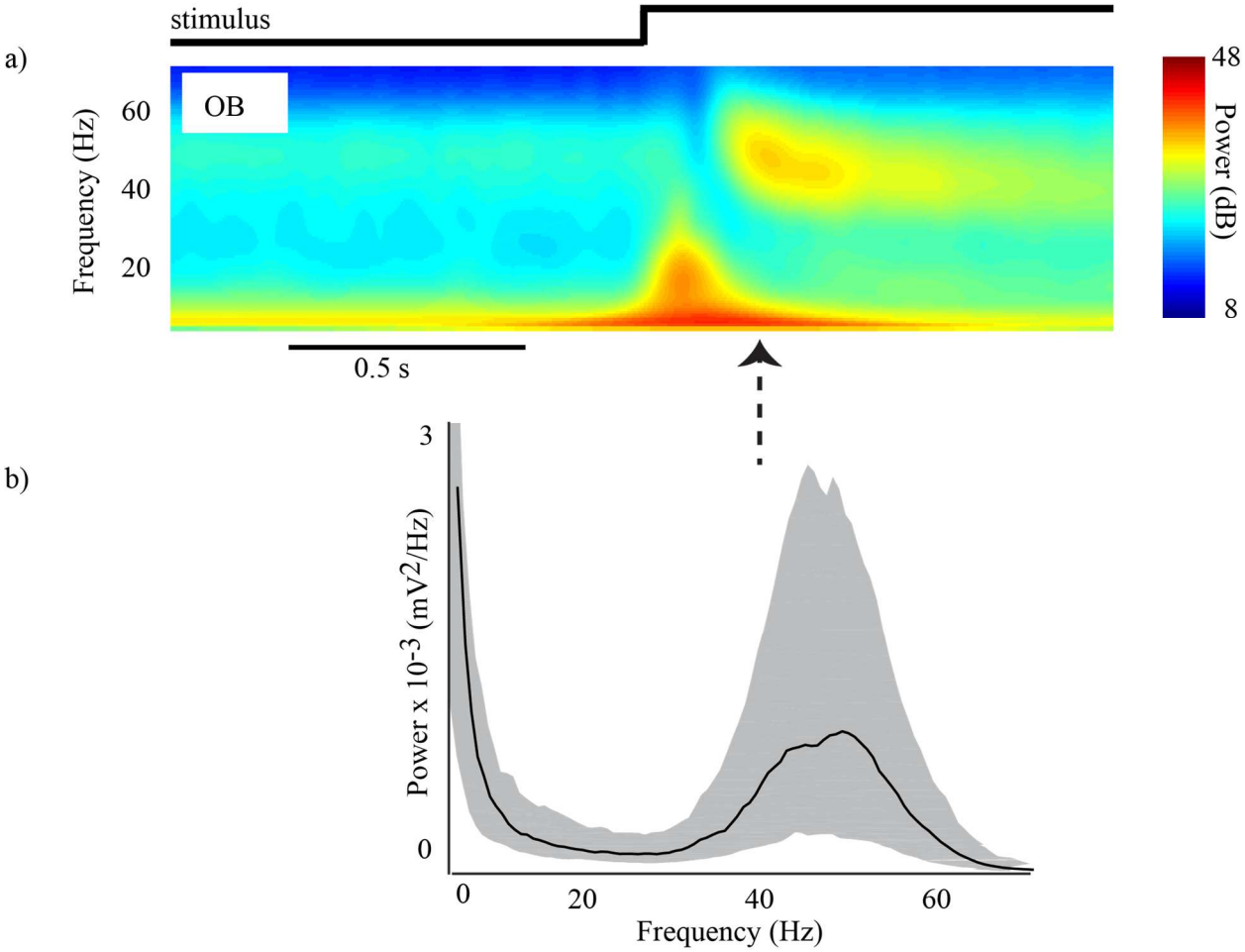

Figure 17: a) The averaged PSD over all animals and trials and stimuli. B) At a time, t denoted by an arrow we showed the average and the interquartile range giving us the variation.

More gamma oscillations come to existence after the stimulus in a wider variety of frequencies and there were relatively short-lived beta frequencies (near 20 Hz) in the OB. The aPC differed in its frequency contents from OB. To understand the oscillations present we averaged (median) across lots of trials from different trials and animals to get an overall picture. The average PSD is

shown in figure 17 a) and at any time t denoted by an arrow in the figure the interquartile range gives us the variation among the trials.

Measuring directed interactions

Once we have the power spectrum, we know the frequencies elicited in the OB and which frequencies are elicited in the aPC. Our next quest would be to understand the role of different frequencies in carrying signals from OB to cortex and vice versa. There are different measures of connectivity which shines light upon different questions. For example, there are phase-based connectivity measures as well as power-based connectivity measures. However, when which method should be used once again depends on the on the question and the kind of measurements that one has at hand. Phase based connectivity is often guided by the thought that two functionally connected neural networks oscillatory activities should be synchronous. However, the conclusions drawn from such tools need to be analyzed correctly. Phase based connectivity measures like intersite phase clustering are independent of power. If we want to decouple power and want to understand the connectivity it provides a good background. There are other measures such as spectral coherence which considers the power also. There is always the concern of volume conduction for this kind of measurements as activity from a different source might affect both the neural areas and we might get coherence in between these two areas. One way to deal with it is to see if phase lags are 0(or pi) as volume conduction is almost instantaneous, and to eliminate that pseudo connectivity but that increases elimination of actual 0 phase connectivity also. One must make a call in these kinds of scenarios based on the prior knowledge or the hypothesis to be tested.

Here we will use Granger causality which is a test of how much the variance of one variable influences the variances of another variable (and vice versa) to understand the direction of interactions between OB and aPC. The advantages for our case for using it is mainly it gives a directional sense which the previous methods cannot. That is, we can distinguish X to Y influence

from Y to X influence. Granger causality is not as much sensitive to volume conduction as the previous phase-based measures are, but two drawbacks are its sensitivity to nonstationary cases and that it is computationally expensive. The term 'causality' to some sense is misleading as Granger causality does not really establish causality; rather it provides a statistical support for the hypothesis that one time series influences another. It has been used for long time for econometric analysis (Granger 1969) and now has made its way to neuroscience which helps us to understand various connectivity. It is applicable in both time and frequency domain. In the next section we compare Granger causality with the alternative approach provided by coherence and phase locking value.

Coherence and PLV

Phase locking value (PLV) generally is used to detect synchronization of neural activities represented in two channels (Lachaux, Rodriguez, Martinerie, & Varela, 1999). As we have said earlier it is often thought that connected parts if the brain may behave synchronously. Implementing PLV is quite easy. First, we extract the phase information at all time points for both the OB and the aPC $\varphi_1(t)$ & $\varphi_2(t)$ for a particular frequency. We can find this phase or angle information either from our wavelet analysis or we can extract that by Hilbert transforms (the later will give the amplitude information also we can neglect that). Once we have that we can find the phase difference $\Delta\varphi = \varphi_1(t) - \varphi_2(t)$. The idea behind this is if the activities are synchronous then over trial it would be consistent, so it averages up to a significant value over multiple trials. However random phase differences will cancel out.

$$PLV(t) = \frac{1}{\mathrm{N}}\left|\sum_1^{\mathrm{N}} \mathrm{e}^{\varphi_1(\mathrm{t})-\varphi_2(\mathrm{t})}\right|$$

We then do a baseline normalization to see the effects of the stimuli.

Coherence is another phase-based connectivity measure which keeps track of the amplitude which the PLV does not. It can be shown coherence is PLV weighted by the amplitudes of the individual signals at that frequency. This weightage can be thought of as a SNR ratio also.

$$\mathrm{Coh}(f) = \frac{\left|S_{xy}(f)\right|^2}{S_{xx}(f)S_{yy}(f)}$$

Here we show the coherence obtained from few trials in between the OB and the aPC and we will see how much it differs from the PLV. Here we show the PLV and the coherence obtained from few trials. The LFPs weren't filtered.

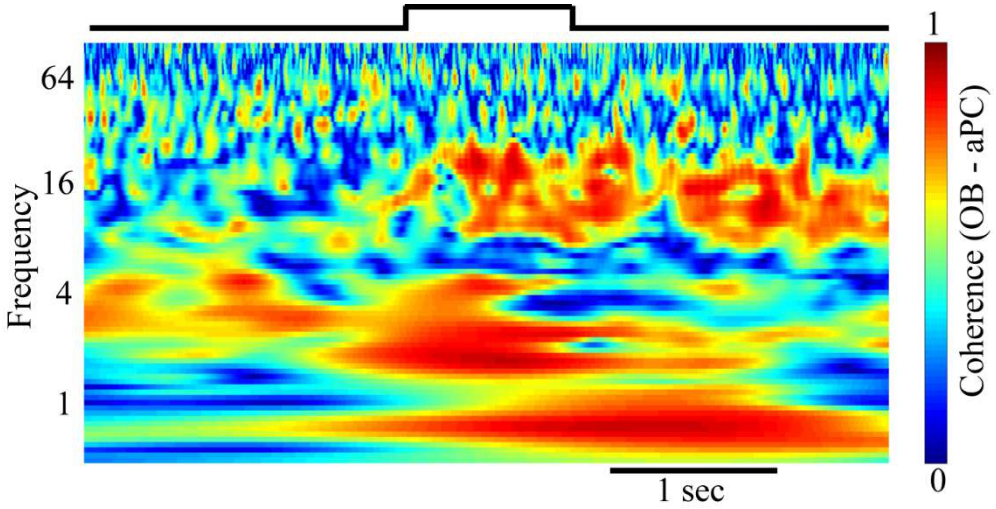

Figure 18: Figure showing the coherence between the OB and the aPC.

We will see(next) in figure 19 how the PLV values are between the OB and the aPC. These are quite patchy however when we use a lot of trials we can see a clearer picture. Both the PLV and coherence are more or less portraying the same picture over here. We see some synchronization around frequencies 16HZ and 50HZ and very low frequencies around 1 HZ. The lower frequency synchronization is bit worrying as we see that our ERP has massive low frequency fluctuations (Fig 5).

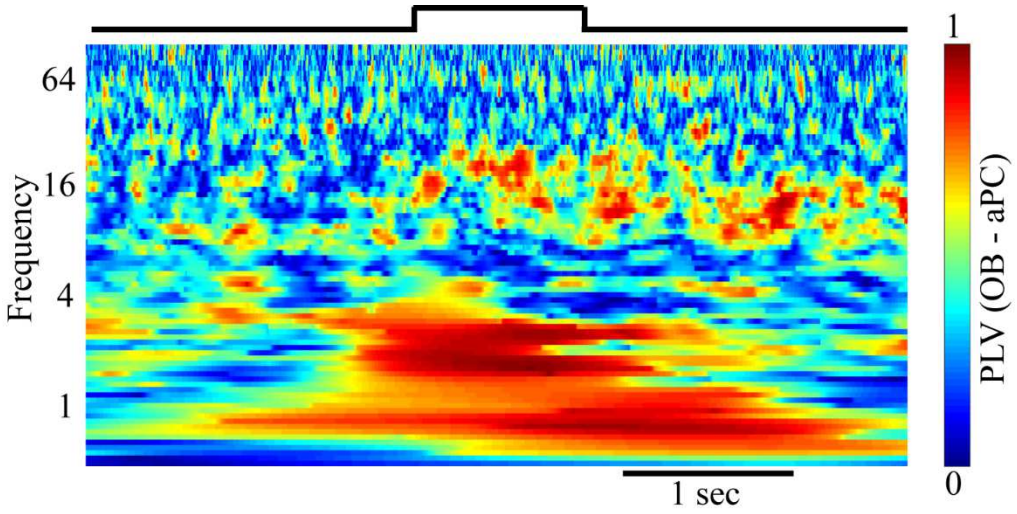

Figure 19: Figure showing the PLV between the OB and the aPC

We couldn't separate between the functional connectivity (which arise essentially from the neural coupling and the stimulus) and the effective connectivity. We subtract the ERP from the individual trial LFPs and we hope that the ERP subtracted LFP will show the actual evoked responses.

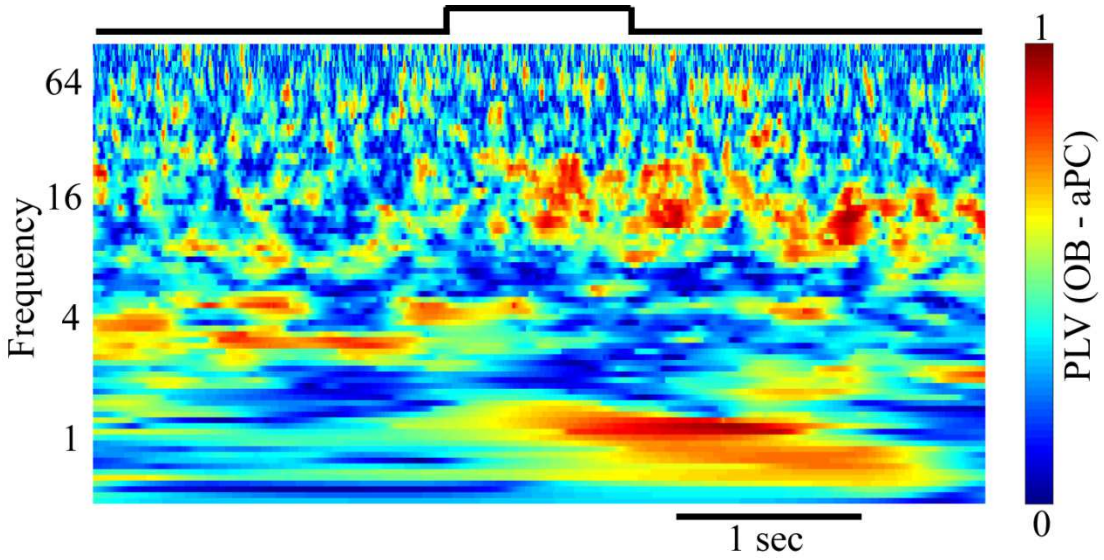

Figure 20: Figure showing the PLV between the OB and the aPC with the ERP subtracted

We see that once we subtract the ERP from the individual trials we can get rid of some of the low frequency synchronizations. We still have some concerns regarding the volume conduction which has zero phase lag and we can eliminate that also by imaginary coherence a measure which remove zero phase lagged synchronies as most of the zero phase lagged synchronies rise from volume conduction. The main drawback of coherence is that it does not provide a direction of influence. Since our goal is to understand feedforward and feedback signal exchange between OB and aPC, we invoke Granger causality, which does provide a measure of the direction of influence.

Granger causality

The main notion of Granger causality is that we can predict one variable based on the information of another variable, if the other variable has a causal influence. Let us suppose we have two variables (time series) X and Y. They can be any time series, for us it's the LFP recordings from the OB and the aPC. If we can predict X better if we know the past of Y we say Y Granger causes X. When we say predict better we mean with statistical support. Or if we find it doesn't we say X is independent of the past of Y, and Y does not Granger cause X. It has a bidirectional sense to it, X can cause Y and Y can cause or not cause X. X to Y and Y to X are not the same thing. This analysis in general can be done over multiple set of variables. However since we are interested only in two (OB and aPC), we will describe the bivariate analysis with 2 variables X and Y. Granger causality is based on vector autoregressive (VAR) modelling. Let us take some time in explaining this. The general autoregression equation, AR(p) is

$$\begin{pmatrix} X_t \\ Y_t \end{pmatrix} = \sum_{k=1}^{p} \begin{pmatrix} A_{xx,k} & A_{xy,k} \\ A_{yx,k} & A_{yy,k} \end{pmatrix} \begin{pmatrix} X_{t-k} \\ Y_{t-k} \end{pmatrix} + \begin{pmatrix} \varepsilon_{x,t} \\ \varepsilon_{y,t} \end{pmatrix} \quad (1)$$

In the above equation we see how the past of the variables (X and Y) are influencing the present, p is the order of the AR process meaning the present is influenced by p time steps back. A's are

the autoregression coefficients and ε's are the residuals or the non-predictable part. Let's define the residual covariance matrix.

$$\Sigma \equiv cov\begin{pmatrix}\varepsilon_{x,t}\\ \varepsilon_{y,t}\end{pmatrix} = \begin{pmatrix}\Sigma_{xx,k} & \Sigma_{xy,k}\\ \Sigma_{yx,k} & \Sigma_{yy,k}\end{pmatrix} \quad (2)$$

So the above process is basically summarized by 2 parameters A and Σ. If we can determine these 2 parameters of the process and the order p we, can describe it successfully.

We see how the X varies as in eqn 1 .

$$X_t = \sum_{k=1}^{p} A_{xx,k} X_{t-k} + \sum_{k=1}^{p} A_{xy,k} Y_{t-k} + \varepsilon_{x,t} \quad (3)$$

So we see how the past of Y has an influence on the present X. However, if there were no influence of Y on X then the A_{XY} coefficients would have been 0. Then the equation would have been

$$X_t = \sum_{k=1}^{p} A'_{xx,k} X_{t-k} + \varepsilon'_{x,t} \quad (4)$$

Then the question comes is which one better represents the data. The error terms help us in this. If our model is better then the error terms will be less, if equation 3 is better than equation 4 the variance in the error terms in equation 3 (ε) will be less than the variance in the error term of equation 4(ε'). Granger causality tests this. If there is some influence from Y to X then obviously eqn 3 will be better suited for us and the error terms (actually variance in the error terms) for equation 3 will be less and the Granger causality test would be

$$\mathfrak{f}_{y\to x} \equiv \ ln\ \frac{|\Sigma'_{xx}|}{|\Sigma_{xx}|} \tag{5}$$

If there were no influences then the error terms would almost be the same and it would be 0 (ln1 =0) .

To assess how interactions between X and Y change over time, the granger causality calculations can be implemented on the data after cutting it into shorter periods. For each short period, we can calculate Granger causality But all this is Granger causality prediction in time domain. As discussed above, we would also like to know if different frequencies of oscillations have different Granger causality.

Next we will show how the Spectral Granger causality unfolds. We will use the same convention and method here as shown before (Barrett, Barnett, & Seth, 2010). For a VAR process the autocovariance sequence Γ_k can be related to the Var parameters (A,∑) by the Yule-Walker equation.

$$\Gamma_k = \sum_{i=1}^{p} A_l \Gamma_{k-l} + \delta_{k0}\Sigma \qquad k = \ldots, -2, -2, 0, 1, 2, \ldots \tag{6}$$

We can solve the Γ_k from (A,∑) and vice versa through these equations. From Γ_k we can get the cross power spectral density (CPSD) denoted by S(λ) where

$$S(\lambda) = \sum_{k=-\infty}^{+\infty} \Gamma_k\, e^{-ik\lambda} \qquad 0 \le \lambda \le 2\pi \tag{7}$$

is the Fourier transform of the autocovariance series. Now the CPSD can be factorized as

$$S(\lambda) = H(\lambda)\Sigma H(\lambda) * \qquad 0 \le \lambda \le 2\pi \tag{8}$$

where H is the transfer function given by

$$H(\lambda) = \left(1 - \sum_{k=1}^{p} A_k e^{-ik\lambda}\right)^{-1} \qquad 0 \leq \lambda \leq 2\pi \tag{9}$$

If we split our S and H as

$$H(\lambda) \equiv A(\lambda)^{-1} = \begin{pmatrix} H_{xx}(\lambda) & H_{xy}(\lambda) \\ H_{yx}(\lambda) & H_{yy}(\lambda) \end{pmatrix} \tag{10}$$

and

$$S(\lambda) = \begin{pmatrix} S_{xx}(\lambda) & S_{xy}(\lambda) \\ S_{yx}(\lambda) & S_{yy}(\lambda) \end{pmatrix} \tag{11}$$

This along with equation 8 gives us

$$\mathrm{S_{xx}}(\lambda) = \mathrm{H_{xx}}(\lambda)\Sigma_{\mathrm{xx}}\mathrm{H_{xx}}(\lambda)^* + +2\mathrm{Re}\{\mathrm{H_{xx}}(\lambda)\Sigma_{\mathrm{xy}}\mathrm{H_{xy}}(\lambda)^*\} + \mathrm{H_{xy}}(\lambda)\Sigma_{\mathrm{yy}}\mathrm{H_{xy}}(\lambda)^* \tag{12}$$

Now we would like the above (the spectral density) equation to split into 2 parts, one which reflects the effect of X on itself and the other which can be interpreted as an influence of Y. Unfortunately, the above equation is not decoupled. We need to transform our variables. We use U

$$\mathrm{U} = \begin{pmatrix} \mathrm{I} & 0 \\ -\Sigma_{\mathrm{yx}}\Sigma_{xx}^{-1} & \mathrm{I} \end{pmatrix} \tag{13}$$

This transformation leaves the Granger causality same but the coupled term $\Sigma_{xy} = 0$, so we can decouple the equation without changing the granger causality. Following the above scheme, we come to the following equation where the CPSD gets split into its own spectral

$$\mathrm{S_{xx}}(\lambda) = \mathrm{H_{xx}}(\lambda)\Sigma_{\mathrm{xx}}\mathrm{H_{xx}}(\lambda)^* + \mathrm{H_{xy}}(\lambda)\Sigma_{\mathrm{yy}}\mathrm{H_{xy}}(\lambda)^* \tag{14}$$

terms plus the causal term. So the spectral Granger causality at a frequency λ can be defined as

$$\mathrm{f_{Y\to X}}(\lambda) = \mathrm{l\,n}\left(\frac{|\mathrm{S_{xx}}(\lambda)|}{|\mathrm{H_{xx}}(\lambda)\Sigma_{\mathrm{xx}}\mathrm{H_{xx}}(\lambda)^*|}\right) \tag{15}$$

We can transform it back into untransformed variables which is

$$f_{Y\to X}(\lambda) = \ln\left(\frac{|S_{xx}(\lambda)|}{\left|S_{xx}(\lambda) - H_{xy}(\lambda)\{\Sigma_{yy} - \Sigma_{yx}\Sigma_{xx}^{-1}\Sigma_{xy}\}H_{xy}(\lambda)^*\right|}\right) \quad (16)$$

we can follow the above scheme to find the Granger causality in the frequency domain. As a check it can be shown that the total Granger causality across all frequencies is same as the time domain.

$$\frac{1}{2\pi}\int_{-\pi}^{\pi} f_{Y\to X}(\lambda)\,d\lambda = \mathcal{F}_{y\to x} \quad (17)$$

First, we determine the order p for the VAR process then we estimate the parameters of the VAR (A,Σ) and from which we can find out Γ,S,H using the above equations to find the frequency Granger causality. We used the MVGC Matlab toolbox by Barnett and Seth (2014) for our spectral Granger calculations.

Order selection: The first thing to determine was the model order. The analysis was done on a 1 second time window that was slid by a stepsize of 0.1 secs. The model order depends on the sampling rate. We downsampled our data from 30K Hz to 300 Hz. This reduces the model order and smaller model orders are not very much susceptible to noise. However small model orders fail to detect longer time scale (low frequency activities) interactions. Here we will be interested in above 12 Hz interactions. When displaying Granger spectra time series, the representative time point for the window is chosen to be the end of the window. Here in figure (21) we show three symbolic windows (of different colors) of same size. We do the granger predictions for them and plot each Granger spectrum at the time point at the end of the window.

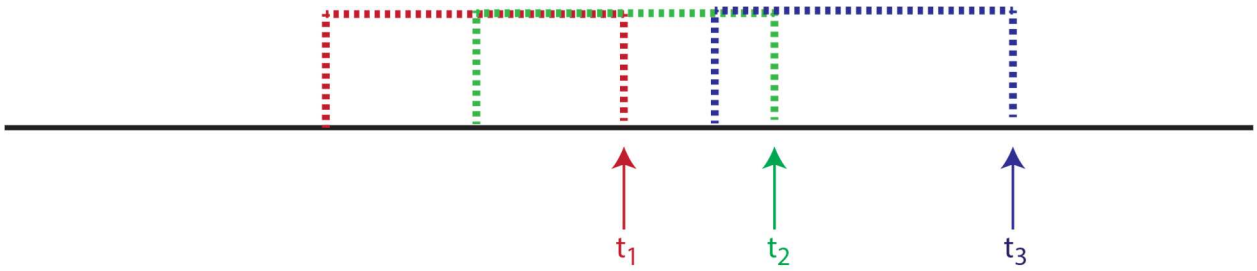

Figure 21 : The spectral Granger causality was measured for a time window and the time point at the end of the window was associated with the measured Granger causal spectra. Here we have shown 3 windows red green and blue with their respective end points as t_1,t_2 and t_3. The Granger spectra from the windows were associated with the time points t_1,t_2 and t_3 and was plotted accordingly to get the time resolved Granger causality plot.

Any analysis based on VAR methods requires a good choice of the model order p. There are various ways the order can be chosen in an automated way. The Akaike Information criterion (AIC) can be used to estimate the model order. The idea is to pick up the model order for where the AIC is the minimum. However, for our data, most of the windows analyzed using the AIC didn't show any local minimum; it usually decreased monotonically. The GC predictions using a model order of p = 15, 20 and 25 were similar and AIC was similarly low for this range of p. So we made the maximum model order to be 20(~ 67 ms) if there weren't any minimum for the AIC. After this we used the MVGC toolbox to estimate the parameters (A,Σ) and the spectral Granger causality (GC) was estimated. Instead of using a single window we used various similar windows to realize it. In Figure 22 we show a single example of the frequency domain GC for our OB and aPC data. We see that most of the GC from the OB to aPC was in the 50 Hz regime whereas there is no such influence on the other way i.e. from aPC to OB.

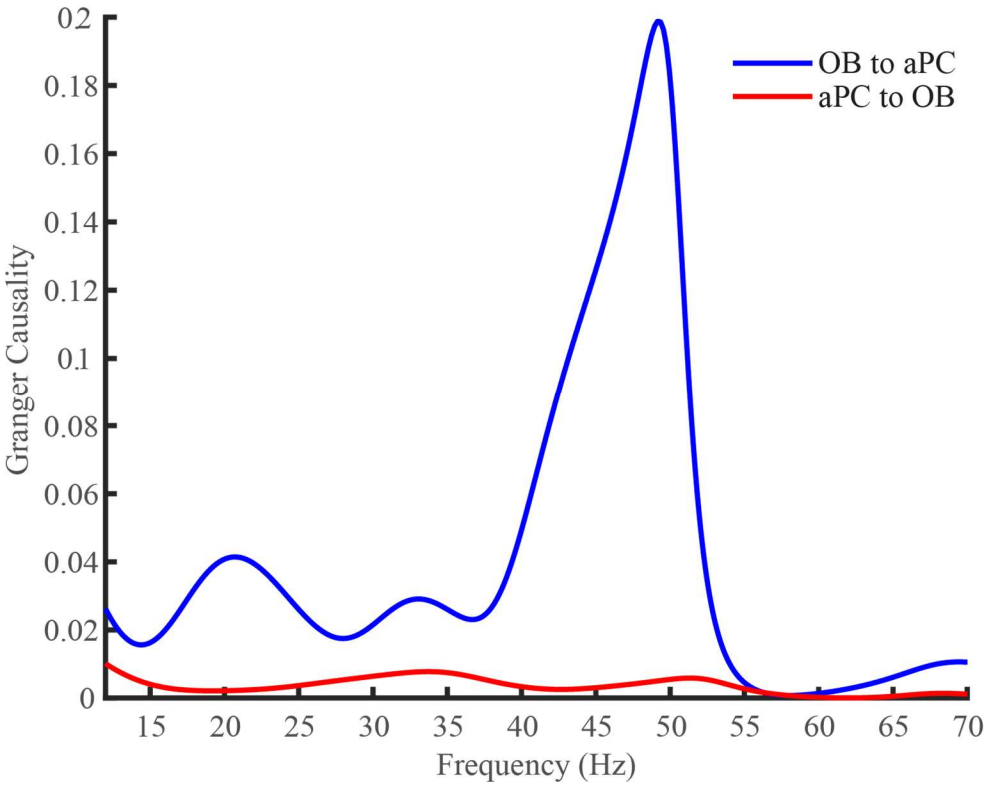

Figure 22: Two Granger causality spectra of OB and aPC. This spectrum was based on a 1 sec window. The trial was for 30 secs so there were 30 one sec windows (ntrials=30) which were used to get the spectra.

When we said we used many similar windows we meant the windows should have the same stochastic underlying mechanisms. We used 10 identical windows which are selected from 10 consecutive stimuli in a trial where it can be assumed that the underlying mechanisms is not changing much. We took windows from identical situations i.e. if are going to analyze window 5 secs before the stimuli we took 10 windows all 5 sec before the stimuli from 10 different but consecutive stimuli and then we used those 10 windows to calculate the GC for 5 secs before the stimuli. There are some concerns as Grange causality calculations, in general, are susceptible to problems due to non-stationarity of the data. In fact, these stationarity issues were more abundant during the onset of the stimuli. We eliminated those windows (which are mostly at the onset of the stimuli) where we failed to calculate the GC.

The Granger spectrum in Fig 22 is based on a one sec window Next, in Fig 23, we show how the Granger spectrum changes over time when a stimulus is presented (defined by 10 consecutive similar stimuli).

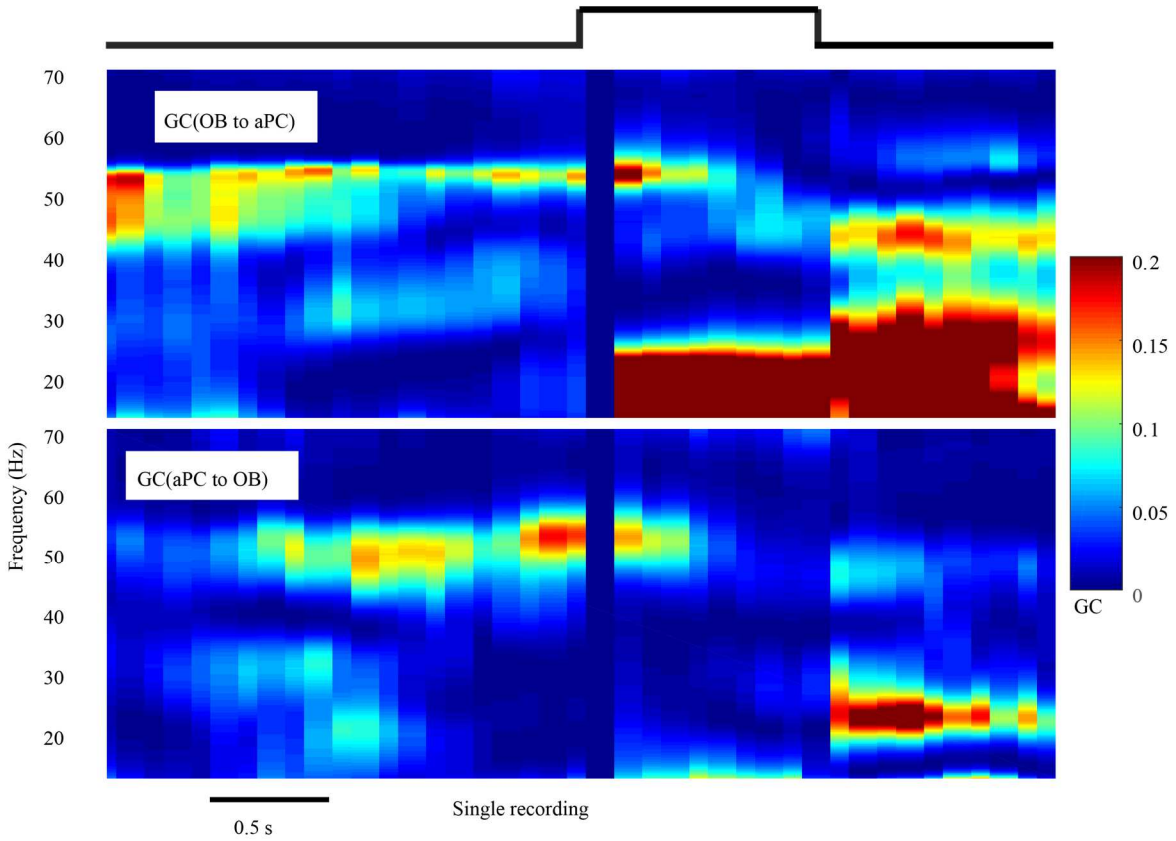

Figure 23: Time resolved spectral granger causality for OB to aPC (top) and aPC to OB (bottom). Time advances along the horizontal axis of these plots. The black line at the top indicates when the olfactory stimulus is on. Color represents Granger causality (GC).

In Fig 23, we see the differences between the GC in the OB-to-aPC direction and the aPC-to-OB direction, during the ongoing activity (before stimulus) and during the stimulus evoked activity. In this example, the algorithm failed to calculate granger causality just at the onset of the stimulus (continuous GC=0 (blue) vertical ribbon) because of nonstationary issues.

The next important step in our GC analysis is to understand the statistical significance of the results. Here, the goal is to quantitatively determine how big GC would be by chance, when there is no real interaction between OB and aPC. If the measured GC is greater than the chance-level

GC, then we may conclude that it is statistically significant. Recall that each Granger spectrogram like that shown in Fig 23 is based on 10 stimulus presentations.

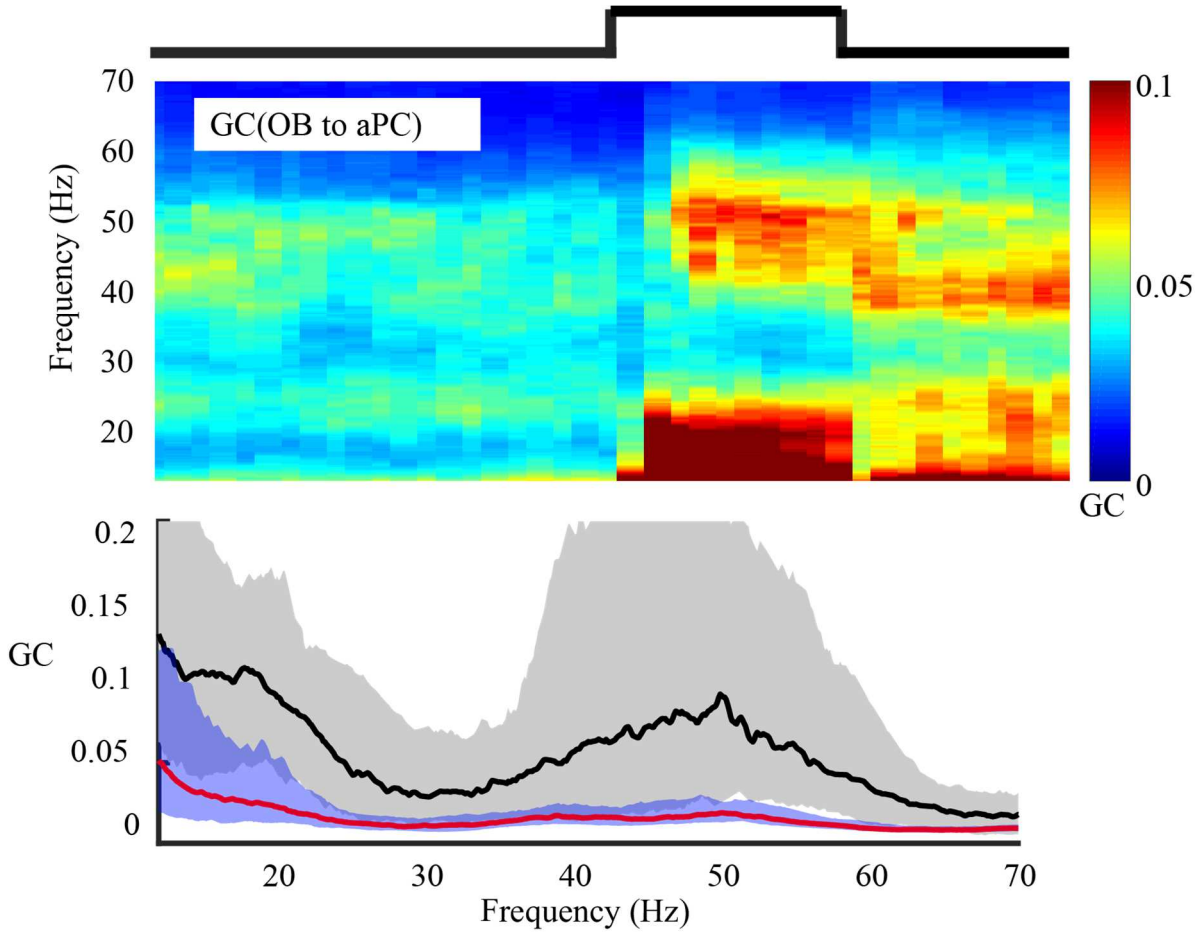

Figure 24: a) The average spectral granger causality spectrogram for OB to aPC for all animals. b) The average GC spectrum for a particular time point along with the interquartile range for both the actual granger causality (black and gray) and the chance-level GC computed from shuffled data (red and blue). The solid line represents the average across animals. The shaded band represents the interquartile range of variation across animals.

To determine the chance-level GC, we randomly permutated the order of the 10 stimuli for OB, but not for aPC. For this randomized data, there will be no real interactions (except those that are consistent for all the 10 stimuli). We repeated this randomization 20 times and then we calculated the granger causality from these permutated series. By comparing the real GC to the twenty chance-level values, we were able to show that the real GC was statistically significant.

Results

In the following results, we will first discuss and present power spectra and power spectrograms, which show which oscillations are present at which times and which locations. Second, we will discuss and present Granger spectra and spectrograms, which reveal the directionality of the interactions between OB and aPC at different frequencies and different times. Finally, we will discuss how these results depend on inhibition in OB, based on the results of pharmacological manipulation of inhibitory signaling.

Power spectra

There were oscillations of various frequencies in the Ob and the aPC. Their patterns changed with time and stimulus. If we concentrate our attention to a single trial, we see the power spectrogram is very patchy. In fact, in a single trial the different oscillations don't go on continuously and they appear sporadically for a small amount of time (Fig 5A). So its quite natural to be patchy as we see here in the spectrogram of a single trial shown in fig 25 a) . We see during the ongoing activity there are bursts of activity in the OB in the gamma band (40 – 60 Hz), but they become more consistent, powerful and longer lasting during the stimulus. We also saw some elicited oscillations around 20 Hz during the onset of the stimulus. But since its so patchy from a single trial its quite difficult to access the trend. We averaged over all the trials and animals to better reveal the signals that are consistent across trials and animals. We find there is a mild gamma oscillation ongoing activity. However, this gamma oscillation becomes significantly more powerful once the stimulus begins and then gradually decreases with time. In aPC we find a similar situation for the low frequencies (approximately near 20 Hz). The onset of these frequencies are bit delayed. It starts 100 ms after the high OB gamma power appears. The high gamma power becomes weaker with time as the low frequency oscillation in the aPC (20Hz) starts to get stronger. The time scale of this delay is consistent with an explanation of

this phenomenon based on Predictive coding Theory . (Wacongne, Changeux, & Dehaene, 2012). In this view, the high frequency oscillation in OB might be carrying the sensory feed-forward signals from the OB to the aPC whereas the low frequency oscillation in aPC might be the negative feedback (which can start only after the feedforward) from aPC that suppresses the OB signal. To test this idea more directly requires connectivity analysis to find the directional influence in between the OB and the aPC.

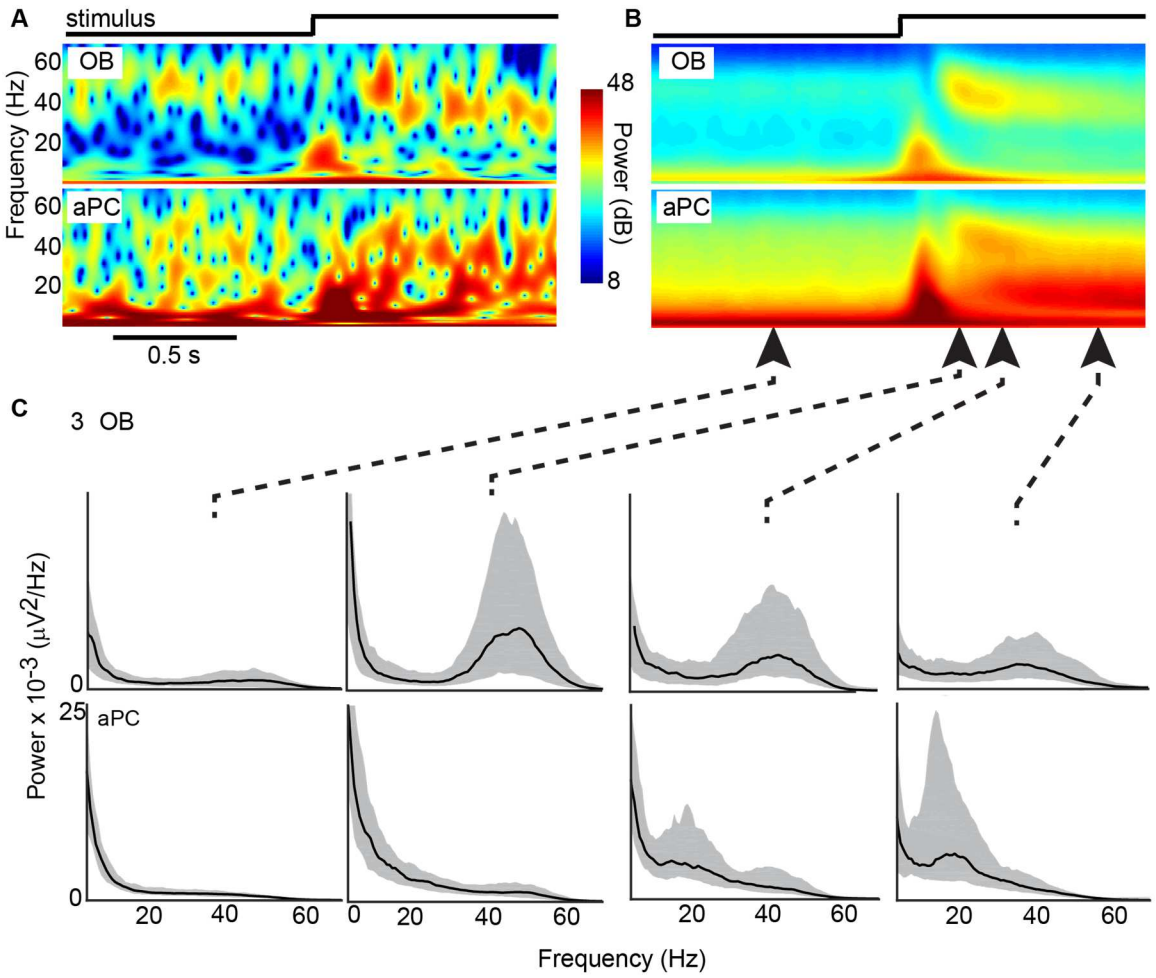

Figure25. Gamma and beta oscillations in the OB and the aPC a) Example, single trial spectrograms show the high frequency (~50 Hz) response in OB (top) and more broad band response in aPC (bottom). b) Trial-averaged spectrograms show us the overall trend. c) Power spectra for four distinct time points indicated by the arrows. Black line represents the mean across trials; gray shaded region defines the interquartile range.

We first show connectivity measured based on the PLV. We see here in figure 26 the PLV obtained by averaging all the trials. Here we do see some definite areas where there are synchronies in the oscillations of the OB and aPC, but they cannot give us any directional sense. They share the synchronous frequencies at time as we expect from our observations from the psd.

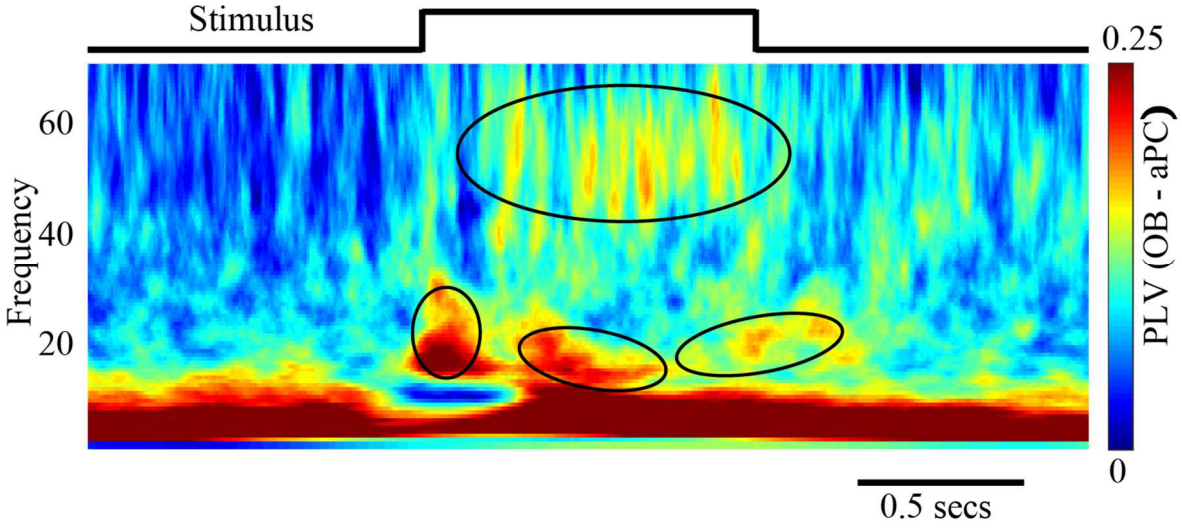

Figure26. PLV between the OB and the aPC showing the synchronous oscillations shared by the two brain areas. Synchronous activities are outlined by the black ellipses.

Granger spectra

To get the directional sense we employ the spectral Granger causality methods (Barnett & Seth, 2014). We show in figure 27, initially there is a high Granger causal influence around frequency 50Hz from the OB to the aPC. There is also aPC-to–OB Granger causal influence, but it starts later and at a relatively low frequency (~20Hz). These observations support our previous speculation that feedforward signals are carried by high frequencies from OB to the aPC whereas low frequency channels are used for feedback signals, consistent with predictive coding theory. There are significant influences also in the lower frequencies (~ 20 Hz) from OB to the aPC continuing till the late response times. If we see the PSD we find that the power associated with these frequencies are relatively weak. So the most prominent OB-to-aPC

influences or interactions are in the high frequencies only. These findings are statistically significant (see Data Analysis section).

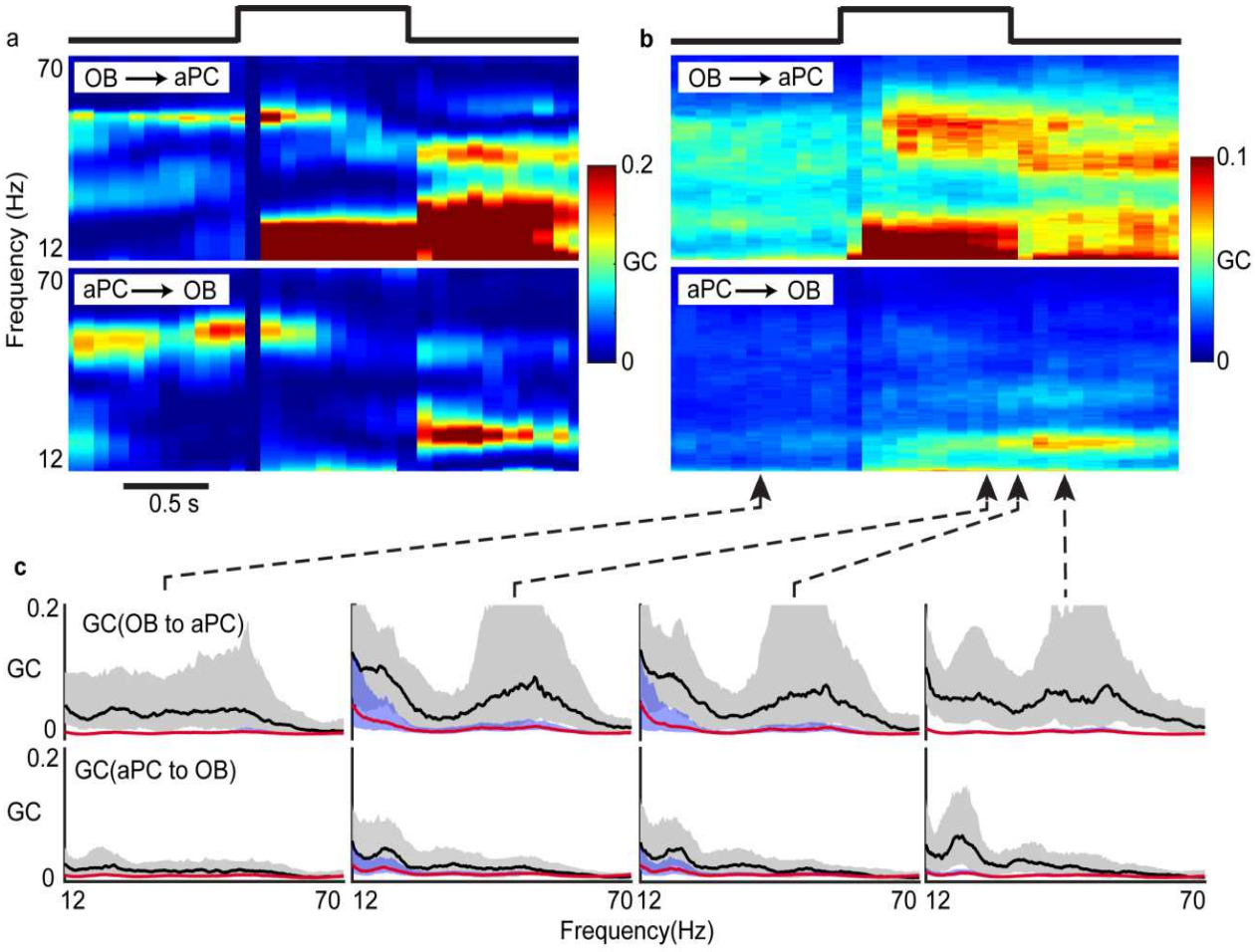

Figure 27. Granger causality showing the feedforward and the feedback signals. a) Single trial Granger causality spectrograms for OB-to-aPC (top) and aPC-to-OB (bottom). b) Trial-averaged Granger spectrograms. There are early feed forward response (significant OB-to-aPC GC, no aPC-to-OB GC) and little delayed feedback (significant aPC-to-OB GC). Other high GC parts don't have significant power in in the PSD (figure26). c) Granger spectra for four different distinct time points shown by the arrows. Black line indicates median across trials; shaded region defines the interquartile range. The red lines trial-shuffled control Granger spectra the blue shaded region around the red line are the interquartile range of GC obtained from the shuffled data. For most part almost for all of the frequencies the black line representing the actual GC are above the upper quartile of the shuffled data indicating the significance of that.

Effects of manipulating OB inhibition

To understand better the above interactions, we changed the inhibition of the OB. There are evidences that the negative feedback in between the mitral/tufted cells and granule cells produce the gamma oscillations in the OB(Eeckman & Freeman, 1990; Kay, 2014). In fact even after a lesion to cut the lateral olfactory tract (LOT) the gamma power in the OB remains the same but it obliterates the beta power (Neville & Haberly, 2003). Our aim was to change the inhibition which will change the gamma power in the OB and hence we can modulate the feedback and the feed forward interactions of the OB and the aPC. To test this we applied $GABA_A$ agonist and antagonist to change the inhibition. We used a signed Kolmogorov Smirnov test to see if the drugged and the no drug responses are statistically different. We summed up all the PSD and GC values within a time-frequency window as a representative of that window and compared with the drugged and the no drug cases. The windows are as follows.

		Time(secs)	Frequency (HZ)			Time(secs)	Frequency (HZ)
PSD	OB	0.23 – 0.43	36 - 55	GC	OB to aPC	0.23 - 1.4	36 - 55
	aPC	0.65 – 1.25	10 – 23		aPC to OB	0.5 – 1.6	12 - 23

Table1 : Time frequency windows (relative to stimulus onset) for GC and PSD used for the KS test to test statistical significance of changes in GC and PSD caused by drug manipulation of inhibition.

We can see the results in figure 28. $GABA_A$ agonist Muscimol (20 μM) reduces the stimulus evoked gamma power in OB $p<0.02$ for 3 out of 4 rats, two-sample Kolmogorov-Smirnov test,

Fig 28a). However, this didn't reduce the corresponding high frequency feedforward GC during the stimulus period. $GABA_A$ antagonist bicuculline (20 μM) increased gamma power in the psd ($p<0.02$ for 4 out of 5 rats, Fig 28c) and also for the feedforward GC ($p<0.02$ for 2 out of 5 rats, Fig 28d) during olfactory stimulation. Changing the OB inhibition also changed the low-frequency feedback.

Figure 28: OB inhibition reduces both feedforward and feedback signals between OB and aPC. a) Trial-averaged spectrograms after applying $GABA_A$ agonist Muscimol in OB reveal weaker high-frequency (~50 Hz) response in OB (top) and decreased the lower frequency power in aPC (bottom). b) Trial-averaged Granger causality though expected to reduce with application of Muscimol remained largely unaffected. c) $GABA_A$ antagonist bicuculline resulted in increased trial-averaged power and (d) Granger causal influence increased for both feedforward and feedback frequencies.

Bicuculline increased the low-frequency power in aPC ($p<0.006$ in 3 of 5 rats, Fig 28c) and made the low frequency feedback (GC) stronger during stimulation ($p<0.02$ in 4 of 5 rats, Fig 28d). Muscimol reduced the low frequency aPC power ($p<0.0002$ for 3 in 4 rats, Fig 28a) in aPC but it didn't change the feedback significantly.

Discussion

We have demonstrated how different frequency bands carry different signals between the OB and the aPC. High frequency gamma band oscillations around 50 HZ carry signals forward from OB to aPC whereas low frequency signals around 20 HZ carries the feedback signals. The feedback and the feedforward also get modulated by changing the inhibition in the OB. Our study also shows a clear evidence of the Predictive Coding Theory in the olfactory system which to our knowledge wasn't demonstrated anywhere before. Previous findings in visual (A.M. Bastos et al., 2015; André Moraes Bastos et al., 2015; Jensen et al., 2015; Michalareas et al., 2016b; Richter et al., 2017; van Kerkoerle et al., 2014) and auditory (Fontolan et al., 2014) cortical networks show frequency specific feedback and feedforward activities. This together

with our study points that this phenomenon can be an outcome of a more general principle of sensory systems involving different brain regions in the sensory hierarchy.

2nd Project: Optogenetic Feedback Control Pilot Project

Overview

Often during history of mankind, we liked to control the outcomes of certain engineered devices and natural systems according to our wishes. Such systems developed by us are known as control systems. There are many control systems which are used in our day to day life like clothes dryer, temperature control, and cruise control of cars. There are very simple control systems like the clothes dryer, which is devised to rotate at a particular rate and supply a particular amount of heat to dry the clothes. The dryer's control system doesn't take any feedback from the system (here the clothes) which often leads to overdried (burnt) clothes or sometimes wet clothes. So, the system couldn't modulate itself by getting the necessary feedback. These kinds of systems can often be improved by using feedback. For example, a humidity sensor in the dryer could provide a feedback signal to stop the process when the clothes are dry . If we bring feedback, the complexity of control algorithms increases a lot (Dorf & Bishop, 2016). For example, if we set up a temperature controller or a cruise control in a car they always take the feedback to maintain the temperature or run the car at 65 mph. The degree of complexity increases further if we include other environmental inputs. For cars using adaptive cruise controls tends to cruise at a specified speed if everything is fine however if it's in a traffic or something else happens it needs to modulate its speed to provide a safe travel for its occupants. In this second project of my thesis, we will consider control in the context of neural systems.

Many parts of the nervous system employ feedback to improve control. This is particularly obvious in the motor system, in which sensory feedback is used by the brain to improve the control signals sent to the muscles so that we can move about and interact with the world effectively. Feedback is used in many less obvious ways in the brain. We have already seen the importance of feedback in the previous sections where feedforward and feedback together

play an important role in processing olfactory sensory input. For many medical applications it might be desirable to have the activities in an area of the brain at a specified level. For example, in neuroprosthetic sensory devices (e.g. cochlear implants) the goal is to control brain activity in a way that is useful for replacing defective sensory organs. Control and feedback in the brain are quite complex in several scales. Deciding our control parameter itself is a challenge. We try to measure the brain state by various measurements like LFP and EEG or look at some aspects of these measurements like frequency contents. In neuroscience feedback control is being used for quite a long time now(Grosenick, Marshel, & Deisseroth, 2015; Newman et al., 2015; Wagenaar, 2005; Wallach, Eytan, Gal, Zrenner, & Marom, 2011). Close loop deep brain stimulation is used in treating Parkinson's disease(Little et al., 2013; Little & Brown, 2012). In the study presented in this chapter of my thesis, we detected LFP fluctuations in the motor cortex of mice and attempted to control the rate of LFP fluctuation events. In this section we give the details how we used a light to keep the firing rate at a certain level in transgenic mice that are genetically modified to have light-sensitive neurons.

Optogenetic stimulation and closed loop feedback control

When attempting to control brain activity, one challenge is that the brain is always active, even without any input from a control stimulus. This would be analogous to trying make a cruise control system for a car that had a fluctuating leak of fuel into the engine. Taking account of the ongoing activity that persists even without any input to the brain from the outside world, makes the control challenging. The response to a control stimulus can be viewed as a sum of ongoing activities and stimulus-evoked activities (Arieli, Sterkin, Grinvald, & Aertsen, 1996; MacLean, Watson, Aaron, & Yuste, 2005). Thus, there is large variability in the outcome of an applied stimulus, due to the variability of the ongoing brain activity. So, our control system should be built in such a way so that it can quickly modulate itself depending on the outcome. The added knowledge of the ongoing activity of the brain would definitely help us in tuning the control

system better. Once we are aware of this we need to decide what activities we would like to control, how we are going to measure and stimulate. In any closed loop control system, the output is modulated for a purpose after receiving the feedback. The output is often compared to a desired output and the error (difference with the desired output) is fed back to the input to modulate the output.

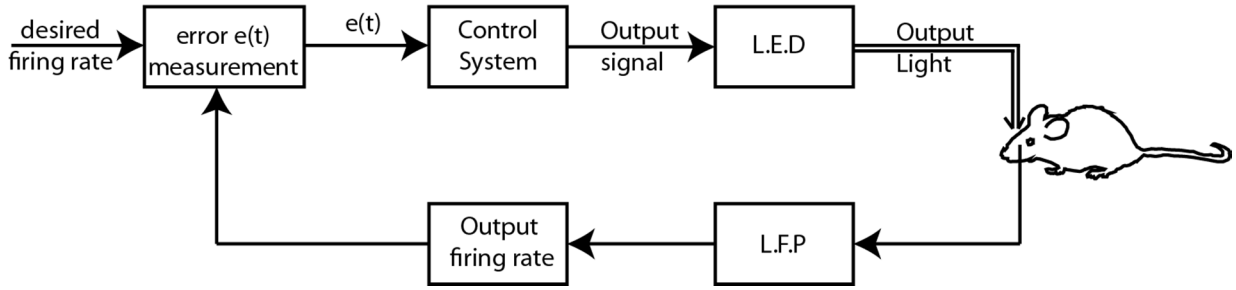

Figure 29: Cartoon representing the above process. A L.E.D light is shunned on the brain of a mouse. The firing rate is measured from the obtained LFP and then is compared with the desired firing rate to get the error which is used to modulate the output signal to the LED.

The system we study here works on this principle. Here we used optogenetic mice for our experiments. These mice are genetically modified to express a light-activated protein in the neurons. The transgenic mice we used had Channelrhodopsin2 (ChR2) (Boyden, Zhang, Bamberg, Nagel, & Deisseroth, 2005; Fenno, Yizhar, & Deisseroth, 2011; Grosenick et al., 2015; Kim, Adhikari, & Deisseroth, 2017)expressed in their neurons. ChR2 is a channel in the membrane of the neuron, which opens when exposed to blue light, which causes transmembrane ion flow and membrane depolarization. A sufficiently bright blue light causes the neurons to fire action potentials. Our aim here is to control and sustain the activity of a large population of neurons at a desired level by tuning the strength/intensity of the light. We would like to modulate the strength of the light based on the feedback from the brain (error).

In this thesis, we present preliminary findings, rather than a completed study. Future graduate students will carry on these experiments based on the foundation of work that we describe here.

Experimental Methods

Subjects

All procedures were carried out according to the recommendations of the Guide for the Care and Use of Laboratory Animals of the National Institutes of Health and was approved by University of Arkansas Institutional Animal Care and Use Committee (protocol #17003). Genetically modified (transgenic) mice Thy1-ChR2-YFP [n=10, female,18±1 gm, B6.Cg-Tg(Thy1-ChR2/EYFP)18Gfng/J from The Jackson Laboratory] were used. These mice express light-activated channel ChannelRhodopsin-2 in the neurons. More details about the mouse are found in the Jackson laboratory website (at the time of writing it is https://www.jax.org/strain/007612). Animals were kept in the animal facilities with proper care. They were housed in a cage of controlled humidity (60%) and temperature (23°C) with 12 h light-dark cycles. The experiments were performed in the light phase.

Anesthesia and surgery

The mice were anesthetized initially using a vaporized form of isoflurane and oxygen gas mixed delivered in a close box. After that the mouse was moved and mounted on a stereotaxic frame and headfixed with two earbars. The mouse was kept in the stereotaxic frame until the end of experiment. The anesthesia gas was delivered to it via a mask put tightly across its snout. The gas/vapor (isoflurane vapor +oxygen) was mixed using an Isoflurane Low-Flow Anesthesia Systems (SomnoSuite, Kent Scientific Corporation). The flowrate was kept at 300mL/min constant throughout all our experiments and the anesthesia percentage was changed according to the need of the experiment. Initially the anesthesia level was kept high(1.5%) while mounting the animal in the stereotaxic table and then lowered till the animal breathes normally. After that the anesthesia level was sustained and controlled according to the needs of the experiment.

A 3mm × 3mm craniotomy was done (1 mm posterior from bregma,3 mm lateral from midline) to access the motor cortex for optic stimulation and recording of neural activity.

Electrophysiology

Neural activity was recorded using a microelectrode array (MEA) (A32, 8 shanks x 4 iridium electrode sites per shank NeuroNexus, MI, USA). Voltages were measured with respect to a ground (AgCl pellet close to the MEA's and it touched the exposed brain surface). Electrodes were inserted to a depth of 650 μm from the surface. The electrodes were lightly tapped to get rid of the brain dimpling effect. The light probe was brought very close to the exposed surface of the brain (at an angle 15 degrees relative to vertical). Care is taken that it doesn't put any pressure on the surface of the brain and should be brought as close possible to it without touching it. The whole adjustments were made under a stereo surgical microscope. Once the optical probe was placed we cover the ground with gelfoams and keep the exposed surface moist with artificial cerebral spinal fluid (ACSF). Care is taken so that the probe is under the ACSF collected in the trough of the craniotomy and no gelfoams or any substance hinders the optical stimulation by displacing the optical fiber or getting in between the optical fiber and the brain which might block the light. Voltages were recorded (digitized) at a 30 kHz sample rate using Cereplex + Cerebus, Blackrock Microsystems (UT, USA).

Optical stimulation

A 470 nm LED (a wavelength suited to activate the ChR2 expressed neurons) was butt-coupled with a 125 µm optical fiber. The optical fiber output is placed carefully not too far way from the MEAs. If we put the light too far away there is a possibility that it will stimulate neurons which the MEA won't be able to pick up. So, the light probe should be placed in a way very close to the MEA (about 1mm away from the point where the MEA penetrates the brain surface) and the angle should be near vertical so that as the light penetrates as deep as possible. Slanting rays

will light up more area on the surface, but the intensity will decrease, and its penetrative power will be lost. We require the light to go as deep as possible since some of the neural activities concerned are at a depth of approximately 400um.. The fiber was attached with a micromanipulator (which was in turn attached to the stereotaxic frame) for minute adjustments. The LED driver was operated in external mode where it is modulated by an external voltage. The external voltage is none other than the feedback determined by the output LFP and was catered to the LED driver by the analog output of the Blackrock Cerebus system. We used MATLAB to process the real time data and give the feedback. It was implemented by a MATLAB code.

Control algorithm

Initially, we set out to measure and control the spike rate of the population of neurons nearby the MEA. However, we found that spikes (action potentials) were difficult to measure in a deeply anesthetized animal. Spikes were more abundant when the anesthesia level was low or the animal was waking up. Since we needed some form of neural activity which was measurable both during high and low level of anesthesia we couldn't go with action potentials. Instead we defined an activity rate based on the LFPs.

First, the raw traces (LFPs) were band pass filtered (10 – 250 Hz). Second, we detected peaks in the fluctuations of this LFP activity. A peak was detected whenever the LFP fluctuates below -30 μV (note that the filtering kept the mean LFP at zero). The activity rate is thus defined as the rate of all LFP peaks recorded from all the 32 recording sites across the MEA. These peaks were recorded on-the-fly by the Blackrock Cerebus system. Then the peak data was accessed by MATLAB (in real time) for feedback processing.

Every 15 ms, the times of all detected LFP peaks were passed from Blackrock hardware to the MATLAB program. The LFP peak activity rates are quite fluctuating with some quick bursts and hence can be quite volatile. We used a moving average (1^{st} order) to smooth out the fastest

fluctuations in the activity rate. We followed the scheme which was previously used for optogenetic feedback control (Newman et al., 2015).

$$f(t) = \alpha r(t) + (1 - \alpha) f(t - dt)$$

Where $r(t)$ is the instantaneous estimate of the activity rate $r(t) = number\ of\ LFP\ peaks/\Delta t$ where $\Delta t = 15\ ms$

The quality of control was sensitive to the choice of the coefficient α. By changing α we are controlling how smooth the activity rates are. A small value of α will smooth out the activity a lot as most of the influence comes from the past term $f(t - dt)$ since its coefficient approaches 1. On the other hand, if we make it large the importance of the past term will be lowered and most of the influence will come from the instantaneous rate which will incorporate fast fluctuations. We tried a range of values and found that $\alpha = 0.01$ worked reasonably well.

Once we have determined the smoothed activity rate $f(t)$ by the above scheme we subtract it from our target activity rate $\tilde{f}$ to get the error $e(t)$. The ultimate goal of the control algorithm will be to minimize the error.

This brings us to choose the target activity rate. The neural circuit we are trying to control is not capable of producing all conceivable activity rates. It is easy to choose a target activity rate that is too high and not possible to achieve. There are various ways to determine or choose what the target activity rate can be. Our strategy was to use the ongoing activity rate during a period with no stimulus to guide our choice of a target rate. Ongoing activity rates vary not only from animal to animal but also varies from minute to minute for one animal. We tried a couple of schemes to set the target rate. We measured the baseline activity before applying any stimulus or control and then set our target activity rate tp be either 4 or 8 times the base rate. The idea behind this is that the response can differ due to the state of the brain. Controlling a target rate of 25 at one brain state is probably different than trying to keep the activity rate at 25 in another brain state. So instead of a flat target rate we chose a target rate based on the activity rate

before any light is switched on hoping that the activity rate from that part somehow indicates the state of the brain.

We also tried a second scheme to choose the target rate based on both the baseline ongoing activity and the response of the system to a brief stimulus. We measured the base rate of ongoing activity like before and then we shine light for a very brief amount of time (1 sec) and see the response and try to keep the target rate somewhere in between. This helps to keep the target rate somewhere reasonable and helps us to keep things in bounds. In the end, we found that a simpler choice of target based only on the ongoing activity rate was more successful.

Once we have got the activity rate and the target activity rate we determine the error $e(t) = \tilde{f} - f(t)$ and deliver the feedback based on this. One of the most used control system are Proportional-Integral-Derivative (PID) Controllers the output of which is given by

$$u(t) = K\left(e(t) + \frac{1}{T_i}\int_0^t e(\tau)d\tau + T_d\frac{de(t)}{dt}\right)$$

where $e(t)$ is the error, and the output has three terms. The first term is proportional to the error, the 2nd term is by integration and the 3rd time by differentiating the error term. Here we only deal with the proportional term ignoring the integral and differentiation part of the feedback. However, we note that the smoothing filter we mentioned above has some history effects that are qualitatively similar to the integral term. One thing should be kept in mind that this is in continuous time however any type of discretization done proper changes should be done. Since we dealt with proportional part only the formula remains unchanged and we replace the variables with the sampled variables but that's not the case for the other two terms. So, the output voltage we used was $V = V + P * e(t)$. The process was implemented in real time at a time resolution of 15ms. The value P the proportionality constant plays an important part as it determines how quickly the output will be able to change. By trial and error, we found that P=0.1 and 0.05 were reasonable values for our control problem.

Results

We set a target rate in between the base rate and the response activity rate. We measured the base rate from the activity (no light involved) and the response rate by shining light for a very brief amount of time. We set the target rate midway between the base rate and the response rate. We see the results below in Figure 30.

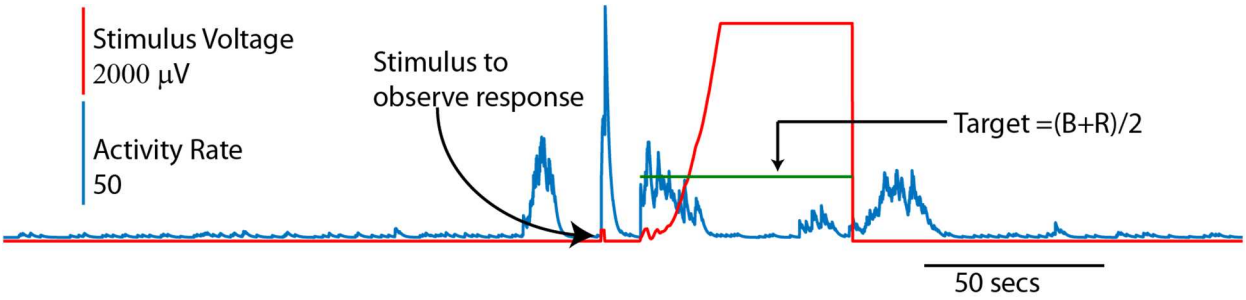

Figure 30: Example of failed control. The base activity rate was measured B, The response rate was measured R ,the target rate (green) was fixed midway between the two. Note that failure entails an activity rate that drops well below the target, even though the stimulus is very intense. This type of 'fatigue' was the most common type of control failure we observed and was challenging to avoid.

The base rate was chosen from 135 secs to 165 secs over 30 secs. And the response was observed only from a short time window of 1 sec 169 secs to 170 secs. The control was started at 180 secs till 240 secs for 60secs. The response was observed to a stimulation of a medium intensity light (250 μV for the control voltage). We see there is quite a large response for our stimulus before the control. In the example shown in Fig 30, our control failed quite quickly after few seconds (5). This example show the typical way that control fails in this system. That is, the neural system becomes 'fatigued' and shows little activity even though the light stimulus is very intense. There can be quite a few reasons for our failure to control well. Perhaps the most likely reason is that if neurons fire too much, they adapt in such a way that prevents further firing. One possibility is that the initial stimulus that we used to define the target rate was

overwhelming and caused some adaptation such that the neurons could not sustain much more activity before becoming fatigued.

So, we changed our strategy and selected the target rate based on the baseline ongoing activity rate only. Now if we see figure 31 we see the activity before control i.e. base rate isn't the same all the time. It had a constant activity but there are some bursts also. That's why it depends on when we choose our base rate. If we make the time period to measure the base rate very short we can end up with a very low activity target rate or a very high target rate depending on where the time window falls. In these scenarios our goal to achieve a reasonable target rate won't be achieved. Again, if we make our window very large it not plausible for various reasons. One it would be computationally difficult but most importantly brain state can change within a very long-time window. We choose a time window of 35 secs (80 to 115 secs) to measure our base rate (B). Then we kept our target rate to be 4B. Below we see how our control system kept the activity rate near our target activity rate. Anesthesia level was maintained by isoflurane at 0.5 %. and P=0.05 for our P controller

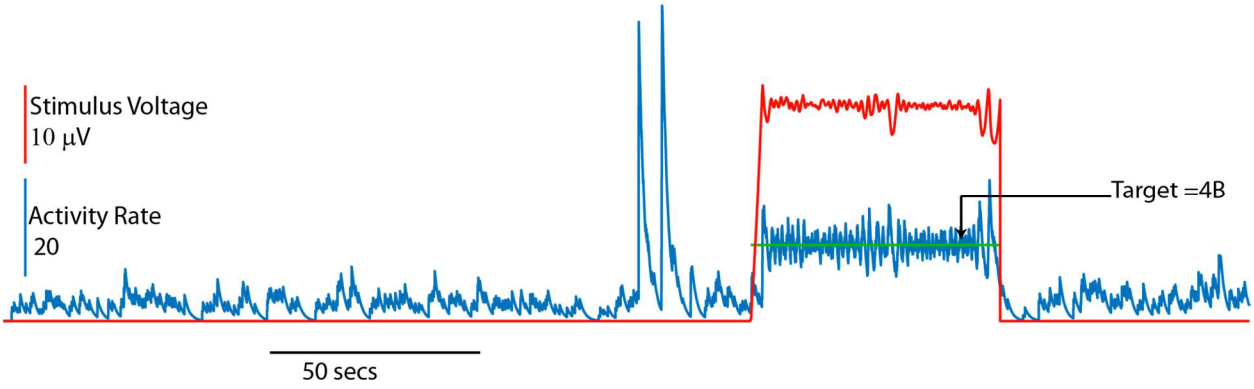

Figure 31: Example of successful control. The base activity rate(B) was measured from 80 to 115 secs, The target was kept at 4B. We found that our control did a reasonable job to keep the activity rate near our target.

We mentioned that brain states change with time. That's a spontaneous change. However, there are other ways to change brain states. We can do that by increasing or decreasing the level of anesthesia. The brain state might or might not change the target rate B. In Figure 31, we

show an example of three attempts of control performed at three different levels of anesthesia. Our question was which level of anesthesia is easiest to control. In this example, we changed the anesthesia level but we kept the target rate fixed instead of being a multiple of the base rate B. We kept the target activity rate to be 90 and changed the anesthesia level (isoflurane levels :0.1,0.3,0.7 %). For anesthesia level 0.1 the control was very good and persistent throughout the 60 secs period control was applied. We see that the output voltage applied fluctuated less and used less power. As we increased the anesthesia level the control went bad and failed prematurely way before the 60 secs period ended. This example suggests that accounting for changes in brain states is important for successful control. Also, we found for higher anesthesia levels that the stimulus voltage (the feedback) increased as per the dictum of our control algorithm but there was no effect on the activity rate and they hit saturation limit very soon. This resulted in more power to keep the activity rate in control at the same specified target level. The base line activity as we can see from figure 32b) decreases with rise of anesthesia level which expected.

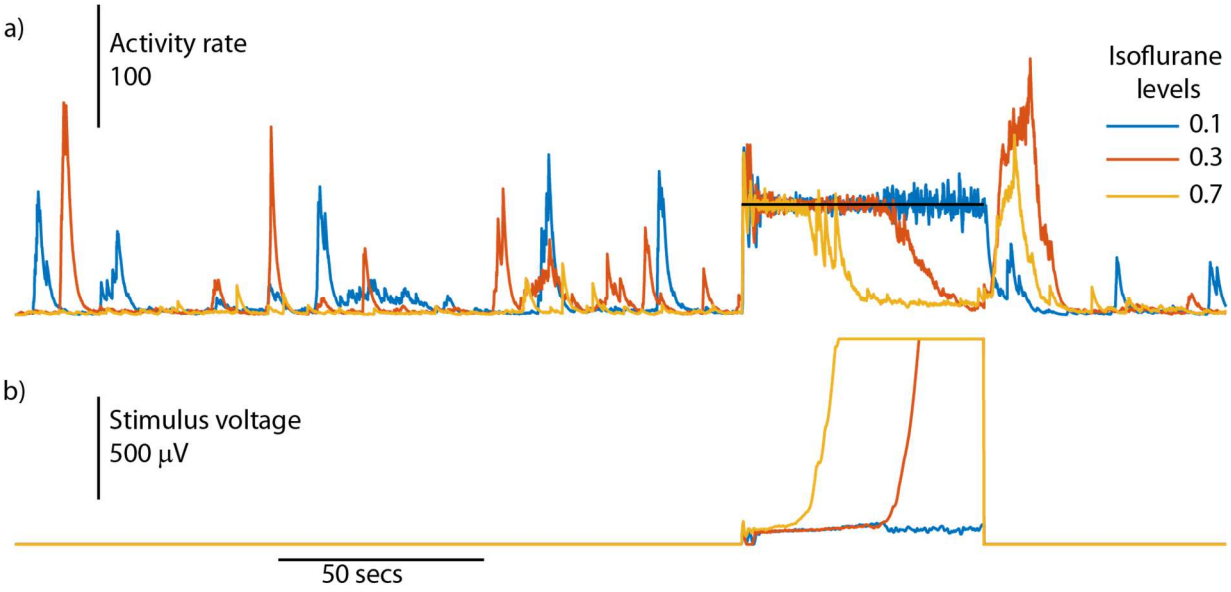

Figure 32: Control under different anesthesia levels. a) The activity rate for 3 isoflurane levels. The lower the isoflurane level the better the control is. b) Controlstimulus time series for the activity rates shown in a.

That's why we should be aware of what questions we are asking while comparing the target rate. If we are interested in how good a brain state is in keeping a target rate for a particular control system, then the target rate should be decided based on the base rate(B). Then we cannot keep a fixed target rate for all the cases. However, if we are concerned how good our control system is doing the job irrespective of brain states and we want to see how our control system perform for various brain states we can fix the target rate like what we have done here.

We noticed for many trials once the control stops a vigorous return of activities occur. This 'rebound' activity is often quite large compared to the base activity or the activity during the stimulus presentation time. We can see that in figure 32a. A moment after the control light stops there is a rebound of activities. We are not very sure about the origin of this activity. This might be a ramification of the saturation of the neurons. We see that in figure 32a for the high isoflurane levels (0.3 and 0.7) the activities get low quickly way before the control stops. The control tries hard but that doesn't help the tired neurons. For these 2 cases we are seeing a great rebound of activities after the control stimulus turns off. In fact 75% of the cases where we observe such surge of activities are saturated because of light. But even if its not saturated there are rebounds. If we see the low anesthesia level trial from figure 32a there is a very small activity (not as large as the other two) which might be thought as a normal burst or activity. However, its time of occurrence is same as the other two which gives us an indication that it might be a similar effect. In that scenario we cannot say its because of neurons has got tired we are seeing the rebound effect, it might be a result of network interactions and not the outcome of a local effect. Further studies are required to determine the cause of the rebound activity following the light stimulus.

Conclusions

We built a control system to keep the activity rate of a population of neurons in mouse motor cortex at fixed target rate. We outline a strategy for how the activity and the target rate could be determined from the LFP measurements. However, this being a pilot project we couldn't come to definite conclusions which require more experiments and data analysis. A few things to try in future studies would be to make the control system better by involving the I and D of the PID controller. We need to quantify the efficiency of our control system and see how the efficiency changes with various parameters. We wanted to see the effect of our control system by changing the state of the brain. We implemented it by changing the anesthesia level. Other methods can be tried to change the state of the brain and observe the effects on the control. If done on awake animals we can set the spike rate as our measurement to control.

Bibliography

Arieli, A., Sterkin, A., Grinvald, A., & Aertsen, A. (1996). Dynamics of Ongoing Activity: Explanation of the Large Variability in Evoked Cortical Responses. *Science*, *273*(5283), 1868–1871. https://doi.org/10.1126/science.273.5283.1868

Barnett, L., & Seth, A. K. (2014). The MVGC multivariate Granger causality toolbox: A new approach to Granger-causal inference. *Journal of Neuroscience Methods*. https://doi.org/10.1016/j.jneumeth.2013.10.018

Barrett, A. B., Barnett, L., & Seth, A. K. (2010). Multivariate Granger causality and generalized variance. *Physical Review E*, *81*(4), 041907. https://doi.org/10.1103/PhysRevE.81.041907

Bastos, A. M., Litvak, V., Moran, R., Bosman, C. A., Fries, P., & Friston, K. J. (2015). A DCM study of spectral asymmetries in feedforward and feedback connections between visual areas V1 and V4 in the monkey. *NeuroImage*, *108*, 460–475. https://doi.org/10.1016/j.neuroimage.2014.12.081

Bastos, A. M., Usrey, W. M., Adams, R. A., Mangun, G. R., Fries, P., & Friston, K. J. (2012). Canonical Microcircuits for Predictive Coding. *Neuron*, *76*(4), 695–711. https://doi.org/10.1016/j.neuron.2012.10.038

Bastos, A. M., Vezoli, J., Bosman, C. A., Schoffelen, J.-M., Oostenveld, R., Dowdall, J. R., … Fries, P. (2015). Visual Areas Exert Feedforward and Feedback Influences through Distinct Frequency Channels. *Neuron*, *85*(2), 390–401. https://doi.org/10.1016/j.neuron.2014.12.018

Boyd, A. M., Sturgill, J. F., Poo, C., & Isaacson, J. S. (2012). Cortical Feedback Control of Olfactory Bulb Circuits. *Neuron*, *76*(6), 1161–1174. https://doi.org/10.1016/j.neuron.2012.10.020

Boyden, E. S., Zhang, F., Bamberg, E., Nagel, G., & Deisseroth, K. (2005). Millisecond-timescale, genetically targeted optical control of neural activity. *Nature Neuroscience*, *8*(9), 1263–1268. https://doi.org/10.1038/nn1525

Bruns, A. (2004). Fourier-, Hilbert- and wavelet-based signal analysis: are they really different approaches? *Journal of Neuroscience Methods*, *137*(2), 321–332. https://doi.org/10.1016/j.jneumeth.2004.03.002

Buzsáki, G., Anastassiou, C. A., & Koch, C. (2012). The origin of extracellular fields and currents-EEG, ECoG, LFP and spikes. *Nature Reviews Neuroscience*, *13*(6), 407–420. https://doi.org/10.1038/nrn3241

Colgin, L. L., Denninger, T., Fyhn, M., Hafting, T., Bonnevie, T., Jensen, O., … Moser, E. I. (2009). Frequency of gamma oscillations routes flow of information in the hippocampus. *Nature*, *462*(7271), 353–357. https://doi.org/10.1038/nature08573

Dorf, R. C., & Bishop, R. H. (2016). *Modern Control Systems* (12th ed.). Pearson.

Eeckman, F. H., & Freeman, W. J. (1990). Correlations between unit firing and EEG in the rat olfactory system. *Brain Research*. https://doi.org/10.1016/0006-8993(90)91663-2

Fenno, L., Yizhar, O., & Deisseroth, K. (2011). The Development and Application of Optogenetics. *Annual Review of Neuroscience*, *34*(1), 389–412. https://doi.org/10.1146/annurev-neuro-061010-113817

Fontolan, L., Morillon, B., Liegeois-Chauvel, C., & Giraud, A.-L. (2014). The contribution of frequency-specific activity to hierarchical information processing in the human auditory cortex. *Nature Communications*, *5*, 4694. https://doi.org/10.1038/ncomms5694

Friston, K. (2010). The free-energy principle: a unified brain theory? *Nature Reviews Neuroscience*, *11*(2), 127–138. https://doi.org/10.1038/nrn2787

Gautam, S. H., Hoang, T. T., McClanahan, K., Grady, S. K., & Shew, W. L. (2015). Maximizing Sensory Dynamic Range by Tuning the Cortical State to Criticality. *PLoS Computational Biology*, *11*(12), e1004576. https://doi.org/10.1371/journal.pcbi.1004576

Gautam, S. H., & Verhagen, J. V. (2012). Retronasal Odor Representations in the Dorsal Olfactory Bulb of Rats. *Journal of Neuroscience*, *32*(23), 7949–7959. https://doi.org/10.1523/JNEUROSCI.1413-12.2012

Gelperin, A. (2006). Olfactory Computations and Network Oscillation. *Journal of Neuroscience*, *26*(6), 1663–1668. https://doi.org/10.1523/JNEUROSCI.3737-05b.2006

Grosenick, L., Marshel, J. H., & Deisseroth, K. (2015). Closed-Loop and Activity-Guided Optogenetic Control. *Neuron*, *86*(1), 106–139. https://doi.org/10.1016/j.neuron.2015.03.034

Helmholtz, H. von. (1924). *Handbuch der physiologischen Optik*. The Optical Society of America.

Jensen, O., Bonnefond, M., Marshall, T. R., & Tiesinga, P. (2015). Oscillatory mechanisms of feedforward and feedback visual processing. *Trends in Neurosciences*, *38*(4), 192–194. https://doi.org/10.1016/j.tins.2015.02.006

Kajikawa, Y., & Schroeder, C. E. (2011a). How local is the local field potential? *Neuron*, *72*(5), 847–858. https://doi.org/10.1016/j.neuron.2011.09.029

Kajikawa, Y., & Schroeder, C. E. (2011b). How Local Is the Local Field Potential? *Neuron*, *72*(5), 847–858. https://doi.org/10.1016/J.NEURON.2011.09.029

Katzner, S., Nauhaus, I., Benucci, A., Bonin, V., Ringach, D. L., & Carandini, M. (2009). Local Origin of Field Potentials in Visual Cortex. *Neuron*, *61*(1), 35–41. https://doi.org/10.1016/J.NEURON.2008.11.016

Kay, L. M. (2014). Circuit oscillations in odor perception and memory. *Progress in Brain Research*, *208*, 223–251. https://doi.org/10.1016/B978-0-444-63350-7.00009-7

Kay, L. M., Beshel, J., Brea, J., Martin, C., Rojas-Líbano, D., & Kopell, N. (2009). Olfactory oscillations: the what, how and what for. *Trends in Neurosciences*, *32*(4), 207–214. https://doi.org/10.1016/j.tins.2008.11.008

Kim, C. K., Adhikari, A., & Deisseroth, K. (2017). Integration of optogenetics with complementary methodologies in systems neuroscience. *Nature Reviews Neuroscience*, *18*(4), 222–235. https://doi.org/10.1038/nrn.2017.15

L.Youngentob, S. (1987). A quantitative analysis of sniffing strategies in rats performing odor detection tasks. *Physiology & Behavior*, *41*(1), 59–69.

Lachaux, J., Rodriguez, E., Martinerie, J., & Varela, F. J. (1999). Measuring Phase Synchrony in Brain Signals. *Human Brain Mapping*, *8*(4), 194–208.

Little, S., & Brown, P. (2012). What brain signals are suitable for feedback control of deep brain stimulation in Parkinson's disease? *Annals of the New York Academy of Sciences*, *1265*(1), 9–24. https://doi.org/10.1111/j.1749-6632.2012.06650.x

Little, S., Pogosyan, A., Neal, S., Zavala, B., Zrinzo, L., Hariz, M., … Brown, P. (2013). Adaptive deep brain stimulation in advanced Parkinson disease. *Annals of Neurology*, *74*(3), 449–457. https://doi.org/10.1002/ana.23951

MacLean, J. N., Watson, B. O., Aaron, G. B., & Yuste, R. (2005). Internal Dynamics Determine the Cortical Response to Thalamic Stimulation. *Neuron*, *48*(5), 811–823. https://doi.org/10.1016/j.neuron.2005.09.035

Markopoulos, F., Rokni, D., Gire, D. H., & Murthy, V. N. (2012). Functional Properties of Cortical Feedback Projections to the Olfactory Bulb. *Neuron*, *76*(6), 1175–1188. https://doi.org/10.1016/j.neuron.2012.10.028

Mazo, C., Lepousez, G., Nissant, A., Valley, M. T., & Lledo, P.-M. (2016). GABAB Receptors Tune Cortical Feedback to the Olfactory Bulb. *Journal of Neuroscience*, *36*(32), 8289–8304. https://doi.org/10.1523/JNEUROSCI.3823-15.2016

Michalareas, G., Vezoli, J., van Pelt, S., Schoffelen, J.-M., Kennedy, H., & Fries, P. (2016a). Alpha-Beta and Gamma Rhythms Subserve Feedback and Feedforward Influences among Human Visual Cortical Areas. *Neuron*, *89*(2), 384–397. https://doi.org/10.1016/j.neuron.2015.12.018

Michalareas, G., Vezoli, J., van Pelt, S., Schoffelen, J.-M., Kennedy, H., & Fries, P. (2016b). Alpha-Beta and Gamma Rhythms Subserve Feedback and Feedforward Influences among Human Visual Cortical Areas. *Neuron*, *89*(2), 384–397. https://doi.org/10.1016/j.neuron.2015.12.018

Neville, K. R., & Haberly, L. B. (2003). Beta and Gamma Oscillations in the Olfactory System of the Urethane-Anesthetized Rat. *Journal of Neurophysiology*, *90*(6), 3921–3930. https://doi.org/10.1152/jn.00475.2003

Newman, J. P., Fong, M., Millard, D. C., Whitmire, C. J., Stanley, G. B., & Potter, S. M. (2015). Optogenetic feedback control of neural activity. *ELife*, *4*, 1–24. https://doi.org/10.7554/eLife.07192

Oswald, A.-M., & Urban, N. N. (2012). There and Back Again: The Corticobulbar Loop. *Neuron*, *76*(6), 1045–1047. https://doi.org/10.1016/j.neuron.2012.12.006

Richter, C. G., Thompson, W. H., Bosman, C. A., & Fries, P. (2017). Top-Down Beta Enhances Bottom-Up Gamma. *The Journal of Neuroscience*, *37*(28), 6698–6711. https://doi.org/10.1523/JNEUROSCI.3771-16.2017

Shipp, S. (2016). Neural elements for predictive coding. *Frontiers in Psychology*, *7*(NOV), 1–21. https://doi.org/10.3389/fpsyg.2016.01792

Spratling, M. W. (2017). A review of predictive coding algorithms. *Brain and Cognition*, *112*, 92–97. https://doi.org/10.1016/j.bandc.2015.11.003

van Kerkoerle, T., Self, M. W., Dagnino, B., Gariel-Mathis, M.-A., Poort, J., van der Togt, C., & Roelfsema, P. R. (2014). Alpha and gamma oscillations characterize feedback and feedforward processing in monkey visual cortex. *Proceedings of the National Academy of Sciences*, *111*(40), 14332–14341. https://doi.org/10.1073/pnas.1402773111

Wacongne, C., Changeux, J.-P., & Dehaene, S. (2012). A Neuronal Model of Predictive Coding Accounting for the Mismatch Negativity. *Journal of Neuroscience*, *32*(11), 3665–3678. https://doi.org/10.1523/JNEUROSCI.5003-11.2012

Wagenaar, D. A. (2005). Controlling Bursting in Cortical Cultures with Closed-Loop Multi-Electrode Stimulation. *Journal of Neuroscience*, *25*(3), 680–688. https://doi.org/10.1523/JNEUROSCI.4209-04.2005

Wallach, A., Eytan, D., Gal, A., Zrenner, C., & Marom, S. (2011). Neuronal Response Clamp. *Frontiers in Neuroengineering*, *4*(April), 1–10. https://doi.org/10.3389/fneng.2011.00003

Appendix

UNIVERSITY OF ARKANSAS

Office of Research Compliance

MEMORANDUM

To: Woodrow Shew

From: Craig Coon, IACUC Chair

Date: August 22, 2016

Subject: IACUC Approval

Expiration Date: August 17, 2019

The Institutional Animal Care and Use Committee (IACUC) has APPROVED your protocol #17003 "Optogenetic dissection of retronasal olfaction" contingent upon your compliance with any stipulations for the use of urethane set forth by the UARK office of Environmental Health and Safety.

In granting its approval, the IACUC has approved only the information provided. Should there be any further changes to the protocol during the research, please notify the IACUC in writing (via the Modification form) prior to initiating the changes. If the study period is expected to extend beyond August 17, 2019 you must submit a newly drafted protocol prior to that date to avoid any interruption. By policy the IACUC cannot approve a study for more than 3 years at a time.

The IACUC appreciates your cooperation in complying with University and Federal guidelines involving animal subjects.

CNC/aem
cc: Animal Welfare Veterinarian

Administration Building 210 • 1 University of Arkansas • Fayetteville, AR 72701-1201 • 479-575-4572
Fax: 479-575-3846 • http://vpred.uark.edu/199

UNIVERSITY OF ARKANSAS

Office of Research Compliance

MEMORANDUM

TO: Dr. Woodrow Shew

FROM: Craig N. Coon, Chairman
Institutional Animal Care and Use Committee

DATE: June 6, 2014

SUBJECT: IACUC APPROVAL
Expiration date: June 30, 2017

The Institutional Animal Care and Use Committee (IACUC) has APPROVED your protocol 14049: "Retronasal olfaction". Your start date is July 1, 2014

In granting its approval, the IACUC has approved only the information provided. Should there be any further changes to the protocol during the research, please notify the IACUC in writing(via the Modification form) prior to initiating the changes. If the study period is expected to extend beyond June 30, 2017 you must submit a new protocol. By policy the IACUC cannot approve a study for more than 3 years at a time.

The IACUC appreciates your cooperation in complying with University and Federal guidelines involving animal subjects.

CNC/aem

cc: Animal Welfare Veterinarian

Administration Building 210 • 1 University of Arkansas • Fayetteville, AR 72701-1201 • 479-575-4572
Fax: 479-575-3846 • http://vpred.uark.edu/199

Request for Modification of an Approved Animal Use Protocol (MR)

IACUC use only:			
Protocol number:	_____	Category(s) of animal use:	
Date Received:	_____	☐ Agricultural	
Approval Date:	_____	☐ Biomedical	
Start Date:	_____	☐ Field	
End Date:	_____	LATA Training Verified	☐ Yes ☐ No

Instructions:

- *This form is required for **any** modifications of an Animal Use Protocol (AUP) which is currently approved by the IACUC.*
  - *Major modifications that would **significantly** change either objectives or design will require a **new** AUP.*
- *In completing this MR, briefly state the Objective(s) of the original approved AUP and how the proposed modification(s) would serve to further satisfy the Objective(s).*
- *Explain the modification(s) so it can be clearly understood how it (or they) fit in the Experimental Design as described in the Approved AUP*
- *It is preferred that this document explain the proposed procedures adequately so that the reviewers do not need a copy of the Approved AUP. However, if necessary refer to the Approved AUP as needed so the reviewers can clearly understand the proposed modification(s).*
- *This is a MicroSoft Word (MSWord) "form". Use MSWord to fill in the information asked for in the blanks ("____") provided. You can put as much information in the blanks as you need to.*

Approved Animal Use Protocol # 14049

Title:

Project Title of Original Protocol: Retronasal olfaction

Start and End Dates of Approved Protocol:

Start Date July 2014 End Date July 2017

Principal Investigator

Name: Woodrow Shew
Department/Division: Physics
Campus Mail Address: 226 Physics Building, Room 242A
Telephone: 479-575-5693
Fax: _____
E-mail: shew@uark.edu

Objective:

- Objective of the Original Protocol: Determine differences between the neural correlates of olfactory stimuli that are inhaled (orthonasal) compared to stimuli that enter the nose via the back of the nasal cavity (retronasal).
- Objective of the Modification: This modification is intented to expand the original study to include rats with genetically modified neurons. The genetic modification expresses light-sensitive channels in specific types of neurons, thus facilitating direct light activation of neurons. This light-activation type of stimulation will be studied together with traditional olfactory sensory stimulation to gain deeper insight on relevant neural mechanisms. All experiments will be in anesthetized rats as in the original protocol. The only commercially available way to obtain these optogenetically modified rats is to breed two lines of rats (CamKIIa-cre and Channelrhodopsin) that are available for purchase from only one company. The resulting offspring are genetically modified as needed.

REQUESTED CHANGES

- **Animals:**
  If applicable:
  - *List any changes in species to be used* - We will add a new strain of genetically modified rats to our study. The only commercially available way to obtain these optogenetically modified

rats is to breed two lines of rats (CamKIIa-cre and Channelrhodopsin) that are available for purchase from only one company. The resulting offspring are genetically modified as needed.

- *List numbers of animals required by this modification* - 30 male offspring (approximately 60 total offspring), 4 breeding animals (2 males, 2 females from each line)

- **Methods:**

  If applicable:

  - *List any changes in Housing* - We will follow standard operating procedures for breeding. The only exception is that we will cull females. The reason for culling the females is that we need to avoid the effects of the estrous cycle on brain activity. For example, it is well established that the neural interactions are strongly modulated by the estrous cycle in rodents. Example references include: 1. Scharfman et al. J Neurosci. 'Hippocampal excitability increases during the estrous cycle in the rat: a potential role for brain-derived neurotrophic factor' 2003 23(37):11641-52) and 2. Galvin and Ninan Neuropsychopharmacology. 'Regulation of the mouse medial prefrontal cortical synapses by endogenous estradiol' 2014 (9):2086-94.
  -
  - *List any changes in Experimental Design (such as treatment agents, procedures, etc.)* -
  - We will add to our previous experimental protocols some steps involving light stimulation of neurons in olfactory bulb and piriform cortex. All of these added procedures will occur after the animal is anesthetized.
  - *List any changes in Non-Surgical Procedures* - _____
  - *List any changes in Surgical Procedures* - _____
  - *List any changes in Euthanasia* - _____

- **Personnel:**

  If applicable:

  - *List any additional personnel that will be involved that are not listed on the Approved AUP, fill in the table below.*
  - *Include any additional qualifications here* → _____

LATA Training Documentation

Person:	*List Names →*	Srimoy Chakraborty	Leila Fakhraei	
Responsibility - PI, Tech, Student, or Other		☐ ☐ ☒ ☐	☐ ☐ ☒ ☐	☐ ☐ ☐ ☐
		PI T S O	PI T S O	PI T S O
Required Modules:				
Base Modules				
The Humane Care and Use of Laboratory Animals	*Date Completed →*	3/31/2013	8/24/2015	____
Policy and Procedures	*Date Completed →*	3/31/2013	7/29/2015	____